Bioactive Materials 8 (2022) 529–544

Contents lists available at ScienceDirect

Bioactive Materials

journal homepage: www.sciencedirect.com/journal/bioactive-materials

Aligned fibrin/functionalized self-assembling peptide interpenetrating nanofiber hydrogel presenting multi-cues promotes peripheral nerve functional recovery

Shuhui Yang [a,1], Jinjin Zhu [a,c,1], Changfeng Lu [b,1], Yi Chai [d], Zheng Cao [a], Jiaju Lu [f], Zhe Zhang [a], He Zhao [a], Yin-Yuan Huang [a], Shenglian Yao [e], Xiangdong Kong [f], Peixun Zhang [b,**], Xiumei Wang [a,*]

[a] State Key Laboratory of New Ceramics and Fine Processing, Key Laboratory of Advanced Materials of Ministry of Education, School of Materials Science and Engineering, Tsinghua University, Beijing, 100084, PR China
[b] Key Laboratory of Trauma and Neural Regeneration, Peking University, Ministry of Education, Department of Trauma and Orthopedics, Peking University People's Hospital, Beijing, 100044, PR China
[c] Department of Orthopaedic Surgery, Sir Run Run Shaw Hospital, Zhejiang University School of Medicine & Key Laboratory of Musculoskeletal System Degeneration and Regeneration Translational Research of Zhejiang, Hangzhou, 310016, PR China
[d] School of Clinical Medicine, Tsinghua University, Beijing, 100084, PR China
[e] School of Materials Science and Engineering, University of Science and Technology Beijing, Beijing, 100083, PR China
[f] School of Materials Science and Engineering, Zhejiang-Mauritius Joint Research Center for Biomaterials and Tissue Engineering, Zhejiang Sci-Tech University, Hangzhou, 310018, PR China

ARTICLE INFO

Keywords:
Peripheral nerve regeneration
Alignment
Nanofibers
Fibrin
Self-assembling peptides

ABSTRACT

Nerve guidance conduits with hollow lumen fail to regenerate critical-sized peripheral nerve defects (15 mm in rats and 25 mm in humans), which can be improved by a beneficial intraluminal microenvironment. However, individual cues provided by intraluminal filling materials are inadequate to eliminate the functional gap between regenerated nerves and normal nerves. Herein, an aligned fibrin/functionalized self-assembling peptide (AFG/fSAP) interpenetrating nanofiber hydrogel that exerting synergistic topographical and biochemical cues for peripheral nerve regeneration is constructed via electrospinning and molecular self-assembly. The hydrogel possesses an aligned structure, high water content, appropriate mechanical properties and suitable biodegradation capabilities for nerve repair, which enhances the alignment and neurotrophin secretion of primary Schwann cells (SCs) *in vitro*, and successfully bridges a 15-mm sciatic nerve gap in rats *in vivo*. The rats transplanted with the AFG/fSAP hydrogel exhibit satisfactory morphological and functional recovery in myelinated nerve fibers and innervated muscles. The motor function recovery facilitated by the AFG/fSAP hydrogel is comparable with that of autografts. Moreover, the AFG/fSAP hydrogel upregulates the regeneration-associated gene expression and activates the PI3K/Akt and MAPK signaling pathways in the regenerated nerve. Altogether, the AFG/fSAP hydrogel represents a promising approach for peripheral nerve repair through an integration of structural guidance and biochemical stimulation.

1. Introduction

Peripheral nerve injury (PNI) caused by natural disasters or traffic accidents leads to serious sensory deficits and impaired motor function, leaving patients with permanent disabilities and severely constraining the development of society [1]. Autologous nerve transplantation, which is commonly regarded as the gold standard for treating large gap PNI in clinic, is hampered by donor site morbidity, limited donor

Peer review under responsibility of KeAi Communications Co., Ltd.
* Corresponding author.
** Corresponding author.
E-mail addresses: zhangpeixun@bjmu.edu.cn (P. Zhang), wxm@mail.tsinghua.edu.cn (X. Wang).
[1] These authors contributed equally to this work.

https://doi.org/10.1016/j.bioactmat.2021.05.056
Received 27 March 2021; Received in revised form 7 May 2021; Accepted 28 May 2021
Available online 12 June 2021

sources, unavoidable size and fascicle mismatch, second incision, and poor functional recovery [2,3]. In addition, the complete recovery rate of autologous nerve grafting is only 50% [4]. Nerve guidance conduits (NGCs) have been extensively investigated by researchers as the synthetic alternatives to nerve autografts, owing to their ability to direct axonal advance and guide nerve growth along the conduit axis [5,6]. However, simple hollow NGCs fail to regenerate large nerve defects with critical sizes (25 mm in humans and 15 mm in rats), which may result in the dispersion of regenerating axons as well as inappropriately targeted re-innervation because of the lack of biological, biochemical, and biophysical cues [7,8]. Therefore, constructing a beneficial intraluminal microenvironment has gained much attention in developing NGCs [9–11].

Various strategies have been employed recently to fabricate NGCs with more complex configurations, for instance, intraluminal fillings, micro-grooves, and multichannels [12–14]. Intraluminal filling materials, including micro/nano fibers, spongy matrix, and hydrogels, resemble the extracellular matrix (ECM) and provide guidance cues for nerve regeneration via constructing an artificial microenvironment [15,16]. However, the functional gap between the regenerated and normal nerves remains a challenge. To obtain optimal repair effects, an ideal intraluminal microenvironment in NGCs is required to possess biomimetic structural features and appropriate mechanical properties to longitudinally guide and support regenerating axons, as well as sufficient permeability to provide trophic support [17–19]. Recent studies have revealed that the synergetic effects of different cues could promote nerve repair [20]. The combination of biomimetic structure and biochemistry guidance cues has more potential to promote neurite eruption, accelerate nerve elongation, and enhance functional recovery in comparison with an individual cue [17,21]. Therefore, we aimed to fabricate a novel filling hydrogel presenting multiple cues that synergistically promote regeneration of large-sized peripheral nerve defects.

The scaffolds with an aligned structure have been demonstrated to positively affect the regeneration of peripheral nerve via enhancing Büngner band formation, Schwann cell (SC) migration, and axon extension [20,22]. Besides, the mechanical properties of the microenvironment have an important influence on cell differentiation, proliferation and migration [23–25]. Soft substrates with stiffness between 10^2 and 10^4 Pa can promote the neurite outgrowth *in vitro*, which is close to the stiffness of nerve tissue [26,27]. Fibrin, a naturally occurring biopolymer, contributes to promoting axonal regrowth in peripheral nerve regeneration [28]. During the process of nerve repair in hollow NGCs, aligned fibrin cables have been reported to form spontaneously within the lumen and bridge the proximal and distal nerve stumps, allowing SCs and fibroblasts to migrate, thereby supporting axonal growth [29,30]. We previously fabricated a three-dimensional (3D) aligned fibrin nanofiber hydrogel (AFG) via electrospinning, which was provided with hierarchically oriented structure from nanoscale to macroscale and low elasticity similar to nerve ECM. The AFG could induce the neurogenic differentiation of stem cells and promote the rapid neurite outgrowth of dorsal root ganglions *in vitro* [31]. Additionally, the AFG was verified to advance axonal invasion and motor function recovery when applied to rat and canine spinal cord injury and 10-mm rat sciatic nerve injury [32–34]. However, AFG lacks biological stimulators that are essential for nerve repair, leading to insufficient nerve regeneration in repairing a long-distance injury.

Biochemical molecules, such as laminin (LN), brain-derived neurotrophic factor (BDNF), nerve growth factor (NGF), and vascular endothelial growth factor (VEGF), also play crucial roles in directing axon elongation, preserving axon survival, and promoting axonal regeneration, which were generally used to modify biomaterials with various methods [35,36]. However, the application of exogenous growth factors is sometimes restricted because of the controversial sources, high cost, and vulnerability [37]. As an alternative, peptide-based materials have shown great promise for biomedical applications [38]. The functional peptide motifs derived from ECM proteins and growth factors were found to mimic their bioactivity in enhancing neurite outgrowth and facilitating cell adhesion, which can be easily combined with self-assembling peptides (SAPs) via solid-phase synthesis [39,40]. The SAPs are generally designed with a hydrophilic side and a hydrophobic side to form stable β-sheet structures via ionic interactions, and the properties can be easily controlled by varying the sequences, peptide concentrations or environmental factors, and incorporating bioactive molecules [41]. In a certain physiological environment, SAPs can form hydrogels with high water content and a nanofibrous network structure analogous with the ECM, and therefore serve as good filling material for NGCs [42]. The typical self-assembling peptide (SAP) RADA16-I (RAD) has been extensively applied in tissue repair with functional motifs including RGD, laminin-derived peptide IKVAV, BDNF-mimetic peptide RGIDKRHWNSQ (RGI), and VEGF-mimetic peptide KLTWQELYQLKYKGI (KLT) [40,43,44]. Additionally, the synergistic application of different functional motifs could be achieved via simply mixing different peptides in various ratios to promote repair effects [45]. As previously reported, a functionalized self-assembling peptide (fSAP) hydrogel comprising synergistic IKVAV and RGI motifs was prepared for nerve regeneration, which promoted Schwann cell adhesion and myelination *in vitro* and facilitated the functional recovery of injured sciatic nerves in rats [46]. Nevertheless, pure SAP hydrogels lack the characteristic aligned morphology exhibited by the nerve ECM.

In this study, we combined AFG with fSAP and successfully obtained an AFG/fSAP interpenetrating hydrogel that exerting synergistic physical and biochemical cues for peripheral nerve regeneration. We fabricated the composite AFG/fSAP hydrogel via electrospinning and molecular self-assembly, and characterized the water content, chemical compositions, microscopic structures, mechanical stiffness, and degradation properties of the hydrogel. The combination mechanism between AFG and fSAP was analyzed via molecular docking simulation, and the morphology and neurotrophin secretion of SCs on the hydrogel were evaluated. The AFG/fSAP hydrogel was then loaded in hollow chitosan tubes to construct tissue-engineered nerve grafts which were used for bridging 15-mm-long sciatic nerve defects in Sprague-Dawley (SD) rats aged 8 weeks. The axonal regeneration and functional recovery were evaluated base on morphological, electrophysiological, and functional parameters. Changes in gene expression and protein levels were assessed for elucidating the molecular mechanism underlying AFG/fSAP hydrogel-induced nerve regeneration.

2. Materials and methods

2.1. Fabrication of AFG/fSAP interpenetrating hydrogel

AFG was prepared via electrospinning as described previously [31,47]. The electrospinning solution containing 2% (w/v) of fibrinogen (F8630, Sigma-Aldrich, Hongkong) and 0.5% (w/v) of poly(ethylene oxide) (PEO, 4,000 kDa, Sigma-Aldrich) in distilled water was electrospun under a voltage of 4 kV. The ejected fibers were continuously collected in a liquid bath with 4 units/mL thrombin (T4648, Sigma-Aldrich) and 50 mM of $CaCl_2$ by a rotating collector (20 cm in diameter) at a speed of 50 rpm (Fig. 1). The electrospun AFG was gathered to form a cylindrical bundle of 1-mm diameter for further use. Then PEO was removed from AFG by washing the fibers with distilled water for 24 h.

The SAP solutions were prepared as reported [46]. The powders of RAD (Ac-RADARADARADARADA-NH_2, purity > 95%, Scilight-Peptide Co., Ltd., Beijing, China), RAD-RGI (Ac-RADARADARADARADA-GG-RGIDKRHWNSQ-NH_2, purity > 90%, ChinaPeptides Co., Ltd., Shanghai, China), and RAD-IKV (Ac-RADARADARADARADA-GG-IKVAV-NH_2, purity > 95%, Scilight-Peptide Co., Ltd.) were dissolved in distilled water (1% w/v), respectively. RAD/IKV/RGI solution was obtained by mixing 25% RAD-IKV solution, 25% RAD-RGI solution, and 50% RAD solution. Afterwards, AFG was immersed in a certain volume of RAD/IKV/RGI solution for 20–30 min to completely

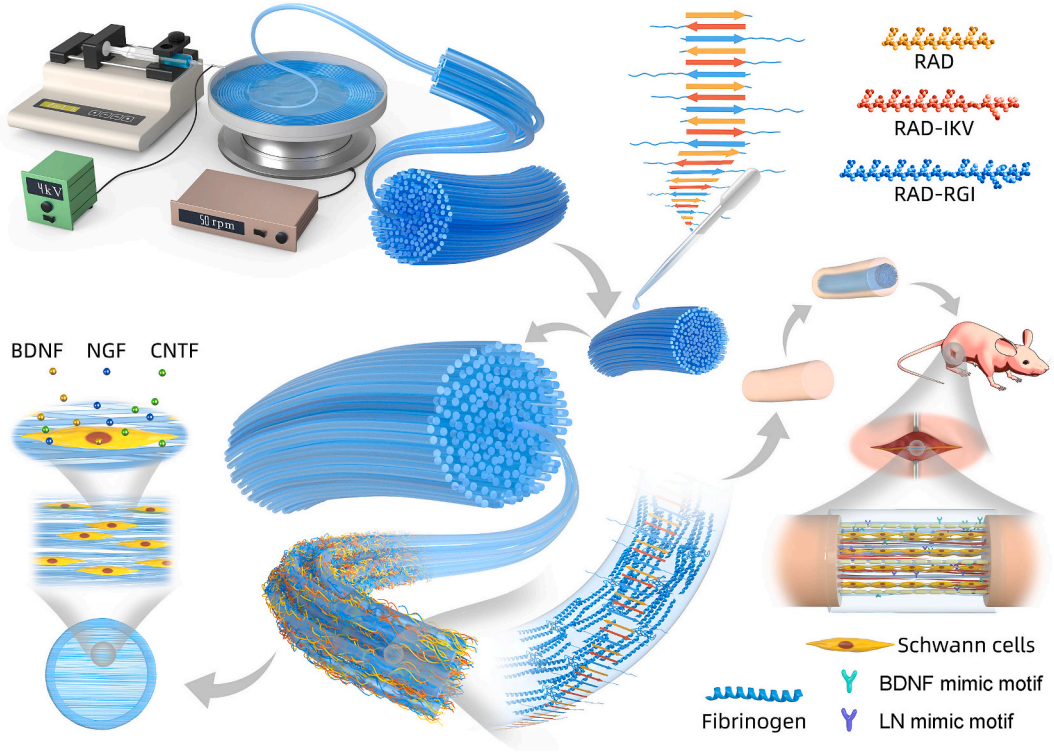

Fig. 1. Schematic diagram of the fabrication of AFG/fSAP interpenetrating hydrogel and the *in vitro* and *in vivo* evaluations. AFG was fabricated via electrospinning with a voltage of 4 kV under a rotating speed of 50 rpm. Functionalized self-assembling peptide solutions were prepared and added to the AFG to obtain the AFG/fSAP interpenetrating hydrogel. The nanofibers of fSAP entangled with the fibers of AFG via molecular self-assembly. Schwann cells cultured on the hydrogel displayed directional morphology and the secretion of CNTF, BDNF, and NGF was upregulated. After implantation to bridge the 15-mm sciatic nerve defect in SD rats, the AFG/fSAP hydrogel promoted axon regeneration and myelination, and facilitated the function recovery after 12 weeks.

absorb the self-assembling peptides, followed by the dropwise addition of phosphate-buffered saline (PBS) or culture medium for equilibrium to obtain AFG/fSAP interpenetrating hydrogel (Fig. 1).

The chitosan conduits were fabricated in accordance with a patent (Patent No. 01136314.2).

2.2. Characterization of AFG/fSAP interpenetrating hydrogel

The weights of the hydrogels were measured before and after lyophilization, and the water contents of the hydrogels were determined using the following formula (n = 3):

$$\text{Water content } (\%) = (\text{Initial hydrogel weight} - \text{dry weight})/\text{Initial dry weight} \times 100\% \quad (1)$$

The freeze-dried hydrogels were ground into fine powders, followed by uniformly mixing with KBr for Fourier transform infrared (FTIR) spectrometry. The FTIR spectrometer (TG-MS-FTIR-X70, NETZSCH Groups, Germany) was used to record the spectra with wavenumbers ranging from 4000 to 400 cm^{-1}.

To observe the microstructure of hydrogels, the hydrogels were fixed with 2.5% glutaraldehyde for 2 h and dehydrated through successive ethanol washes, followed by lyophilization for 24 h. The fiber alignment was evaluated via micro-CT imaging, as described previously [48]. Each sample was scanned using micro-CT (InspeXio SMX-225 CT FPD HR, Shimadzu Co. Ltd., Kyoto, Japan) under the same conditions. Then the morphology of fresh longitudinal sections of the AFG and AFG/fSAP hydrogels was monitored by a scanning electron microscopy (SEM, Carl Zeiss, Oberkochen, Germany). The distribution frequencies of fiber direction in AFG and AFG/fSAP were measured using Image Pro Plus 6.0 (Media Cybernetics, Silver Spring, USA).

To investigate the interaction between fibrin fibers and SAP nanofibers, the hydrogels were observed using a transmission electron microscope (TEM, TECNAI Spirit, FEI, Czech Republic). After fixed in precooled 2.5% glutaraldehyde for 3 h, the AFG and AFG/fSAP hydrogels were further fixed with 1% osmium tetraoxide solution for 1 h. Then the hydrogels were dehydrated and embedded in Epon 812 epoxy resin (Fluka, Münster, Germany). 70-nm-thick transverse ultrathin sections were cut and then stained with uranyl acetate for TEM imaging. The distribution frequencies of fiber diameter and the average fiber diameter in different hydrogels were statistically analyzed using Image Pro Plus 6.0.

Rheological properties of the hydrogels (8 mm diameter, 1 mm height) were measured using an 8-mm diameter parallel plate at 25 °C (Physica MCR301 rheometer, Anton Paar GmbH, Graz, Austria). Storage (G′) and loss (G″) moduli were recorded in a dynamic frequency sweep test (0.010–1.259 Hz at 1% strain).

The stiffness of the hydrogels was measured with an atomic force microscope (AFM, Dimension ICON, Bruker, Billerica, MA, USA). AFM cantilever tips of V-shaped silicon SNL-D probes (nominal spring constant 0.06 N/m) were modified by attaching 20-μm diameter glass beads. The measurement was conducted at 500 points randomly on each hydrogel. The Young's moduli of all hydrogels were determined by fitting the force-indentation plots with the Hertz model.

Molecular docking between fibrinogen and self-assembling peptides was further assessed using ZDOCK software. The fibrinogen crystal structure (PDB ID: 1JY2) was downloaded from RCSB Protein Data Bank. PyMOL 2.3 software was used to construct the SAPs based on the possible structure reported previously [49,50]. The results were assessed in line with the interaction force with each other.

Proton nuclear magnetic resonance (^{1}H NMR) was applied to further verify the molecular interaction of fSAP and fibrin. The fibrinogen and fSAP powders were dissolved in deuterium oxide (D_2O) at a concentration of 10 mg/mL, respectively. Then a 1:1 mixture of the two solutions was obtained for evaluation. The ^{1}H NMR spectra of fibrinogen,

fSAP, and the mixed solutions were recorded on a 600 M NMR spectrometer (JNM-ECA600, JEOL Ltd., Japan) at an ambient temperature.

2.3. In vivo degradation of AFG/fSAP interpenetrating hydrogel

The degradation of the AFG and AFG/fSAP hydrogels *in vivo* was evaluated through subcutaneous implantation and *in vivo* fluorescence imaging system. The hydrogels were immersed in Cyanine5 (Cy5) fluorescent dye solution for 24 h for complete dye adsorption. Twelve SD rats were anesthetized with isoflurane and the dorsal hairs were shaved. The AFG and AFG/fSAP hydrogels with Cy5 were implanted into the dorsal subcutaneous space after incising the back skin of rats. The *in vivo* fluorescence images were acquired using an IVIS 200 small animal imaging system (Xenogen, Alameda, CA, USA) with a Cy5 filter at 1, 4, 7, 10, and 14 days after implantation. The implanted hydrogels and dorsal tissue were harvested from the animals at 7 and 14 days postoperatively.

2.4. Schwann cell morphology and neurotrophin secretion

SCs were harvested and purified from the sciatic nerves of 3-day-old SD rats as described previously [51]. A handcrafted plastic circular ring in 14-mm external diameter, 12-mm internal diameter and 1-mm thickness was utilized as the culturing device for fixing the hydrogels and keeping their aligned features (Fig. 1). The AFG and AFG/fSAP were fabricated to obtain fiber bundles of 1–2 mm in diameter and 30–40 cm in length. Subsequently, the fiber bundles were twined around the circular ring to obtain a flat and aligned substrate for cell culture. The purified SCs were seeded onto the hydrogels at a density of 2×10^4 cells/gel. After 3 days, SCs on the hydrogels were fixed with 4% paraformaldehyde for 20 min and permeated with 0.1% Triton X-100 solution for 5 min, followed by incubation in 10% goat serum for 1 h at 25 °C. Subsequent incubation in primary antibodies against S100 (1:200, mouse polyclonal antibody, Abcam) and p75 nerve growth factor receptor (p75, rabbit polyclonal antibody, Abcam) was performed overnight at 4 °C. After incubation with goat anti-rabbit IgG H&L (Alexa Fluor 594, 1:200, ab150084, Abcam) and goat anti-mouse IgG H&L (Alexa Fluor 488, 1:200, ab150117, Abcam) for 1 h at 25 °C, the nuclei were stained with 4',6-diamidino-2-phenylindole (DAPI) for 20 min, and then imaged using a confocal laser scanning microscope (Leica, Germany).

The CNTF, BDNF, and NGF secretion of SCs on a routine tissue culture plate (TCP), AFG, and AFG/fSAP hydrogels after 3 days was evaluated with enzyme-linked immunosorbent assay (ELISA) kits (Jianglai, Shanghai, China) according to the manufacturer's instructions. A microplate reader (Infinite F50, Tecan, Männedorf, Switzerland) was used to measure the absorbance values.

2.5. Animal procedures

All procedures associated with animals were performed in accordance with the plan approved by the Medical Ethics Committee of Peking University People's Hospital. 44 SD rats (male, aged 8 weeks, 200–250 g) were randomly divided into four experimental groups. The procedures were described previously [42]. A segment of sciatic nerve in the right lateral thigh was resected and removed to leave a 15-mm-long defect. In the Autograft group, the resected nerve segment was reversely re-implanted into the defect. In the Hollow group, both ends of the transected nerve were bridged with an empty chitosan tube. In the AFG and AFG/fSAP groups, the AFG and AFG/fSAP hydrogels were placed into the lumen of the chitosan tubes and implanted to the defects, respectively. All rats were fed with food and water, and monitored for any changes.

2.6. Morphometric evaluation of axonal regeneration

At 12 weeks postoperatively, five rats from each group were euthanized, and the nerve conduits and grafts were retrieved. The distal end of the grafts was cut into 70-nm ultrathin sections and 700-nm semi-thin sections, as previously described [46]. The semi-thin sections were stained with 1% toluidine blue/borax solution and observed using a light microscope (IX81, Olympus, Tokyo, Japan). The average myelinated nerve fiber density of 10 random toluidine blue images in each group was calculated. The ultrathin sections were stained with lead citrate and uranyl acetate, and then observed under TEM (JEOL Ltd., Tokyo, Japan). The thickness of myelin sheaths, the diameter of myelinated nerve fibers, and the g-ratios based on 10 random TEM images in each group were calculated using Image Pro Plus 6.0 software.

2.7. Electrophysiological assessment

At 12 weeks postoperatively, electrophysiological examinations were performed on the re-exposed sciatic nerves at the injury site (n = 5/group). Electrical stimuli (3.0 mA, 1 Hz) were applied to the proximal and distal ends of the nerve graft, and the compound muscle action potentials (CMAPs) were recorded on the belly of the gastrocnemius muscle. The latency and peak amplitude of the CMAPs were compared among the groups.

2.8. Histological evaluations of target gastrocnemius muscle

At 12 weeks postoperatively, the wet weights of gastrocnemius muscles from the injured and contralateral sides of rats were weighed, and the ratio (injured/contralateral) was calculated (n = 5/group). The muscles were fixed in 4% paraformaldehyde at 4 °C for 7 days before embedding in paraffin wax, and cut transversely from the mid-belly to obtain 7-μm-thick sections for Masson's trichrome staining. 10 randomly chosen fields in each sample were imaged and the cross-sectional area of the muscle fibers was quantitatively analyzed using Image Pro Plus 6.0 software.

2.9. Analysis of animal motor function

The motor function was assessed using the CatWalk XT 10.6 gait analysis system (Noldus, Wageningen, The Netherlands) at 2, 4, 6, 8, 10, and 12 weeks postoperatively (n = 5). Data were collected and analyzed, and sciatic function index (SFI) was calculated using a reported formula [45]:

$$SFI = 109.5((ETS\text{-}NTS)/NTS)\text{-}38.3((EPL\text{-}NPL)/NPL)+13.3((EIT\text{-}NIT)/NIT)\text{-}8.8 \quad (2)$$

Evaluations were performed by three investigators blinded to the experimental group.

2.10. Quantitative real-time polymerase chain reaction

At 1 week after surgery, total RNA was extracted from nerve grafts harvested from the rats and reverse transcribed to cDNA, as previous described [46]. Quantitative real-time polymerase chain reaction (qRT-PCR) was performed with a real-time PCR detection system (CFX96, Bio-Rad, Richmond, CA, USA) using iTaq SYBR Green supermix (172–5122, Bio-Rad). Data are expressed as a fold change by using the $2^{-\triangle\triangle Ct}$ method [48]. The sequences of primers used are given in Table S1.

2.11. Western blot analysis

At 1 week after surgery, the nerve grafts were harvested and homogenized in modified RIPA buffer with protease inhibitor cocktail (Mei5 Biotechnology, Co., Ltd., Beijing, China). The protein in the supernatants was quantified and boiled at 100 °C in lane marker loading buffer (CWBIO, Jiangsu, China) for 10 min. A total of 10 μg of protein

from each sample was electrophoresed in SDS-PAGE gels, and then transferred to polyvinylidene fluoride (PVDF) membranes (Millipore, Germany). After blocking with 5% bovine serum albumin (BSA) solution for 1 h at 25 °C, the membranes were incubated with the primary antibodies against phospho-AKT (p-AKT, 1:1000, HUABIO, Hangzhou Huaan Biotechnology Co.,Ltd.), AKT (1:1000, HUABIO, Hangzhou Huaan Biotechnology Co.,Ltd.), phospho-ERK (p-ERK, 1:1000, CST), ERK (1:1000, CST), phospho-p38 (p-p38, 1:1000, CST), p38 (1:1000, CST), phospho-JNK (1:1000, CST), JNK (1:1000, CST), and β-actin (1:1000, Abcam) at 4 °C for 16 h. Subsequently, after incubation with horseradish peroxidase-conjugated secondary antibodies (1:1000, Abcam) for 1 h at 25 °C, the membranes were imaged by a chemiluminescence imaging system (Bio-Rad). Relative protein levels were determined using ImageJ software (NIH).

2.12. Statistical analysis

Each experiment was carried out in triplicate. Statistical analysis was performed with SPSS (v.23.0; IBM corp., USA). Data are presented as mean ± standard deviation (SD), and statistically analyzed using independent *t*-test or one-way analysis of variance (ANOVA) followed by Tukey's post hoc test (equal variances) or Dunnett's T3 post hoc test (unequal variances). A $P < 0.05$ was considered statistically significant.

3. Results and discussion

3.1. Fabrication and characterization of AFG/fSAP interpenetrating nanofiber hydrogel

The aligned fibrin hydrogel was fabricated via electrospinning. The fibrinogen/PEO was ejected from the needle and fell into a liquid bath with $CaCl_2$ and thrombin, enzymatically cross-linking the fibrinogen to form fibrillary fibrin hydrogels (Fig. 1). PEO in the solution contributed to stabilizing the electrospinning, and was subsequently removed by washing the hydrogel in distilled water to obtain pure AFG with strong flexibility and tensile properties [31]. The AFG/fSAP interpenetrating hydrogel exhibited a uniformly transparent appearance, compared to the original white opaque appearance of the AFG under gross observation. The length and diameter of AFG increased marginally after combining with the peptides (Fig. 2A). Based on the same components of AFG and fSAP, the FTIR spectra showed similar characteristic peaks (Fig. 2B). The 1600–1700 cm^{-1} region (amide I) is typically relevant to C═O stretching vibration and associated with the conformation of SAP backbone [52]. The peaks at 1631 cm^{-1} and 1695 cm^{-1} indicated the anti-parallel β-sheet structures in AFG, fSAP, and AFG/fSAP. In the 1480–1575 cm^{-1} region (amide II), the peak at 1541 cm^{-1} reflected β-sheet aggregation in fSAP and AFG/fSAP, directly associated with NH bending and CN stretching, while this peak was absent in AFG, indicating the existence of fSAP in AFG. NH stretching was assessed in the 3100–3300 cm^{-1} region. The spectrum of fSAP showed two peaks at 3080 cm^{-1} and 3291 cm^{-1}, while only one peak at 3291 cm^{-1} was clearly visible in the spectrum of AFG. These peaks were observed at 3070 cm^{-1} and 3291 cm^{-1} respectively in the spectrum of AFG/fSAP, indicating that the combination of fSAP might affect the NH stretching. To investigate the effect of SAP on the alignment of AFG, we scanned the lyophilized hydrogel by using micro-CT and analyzed the orientation of fibers. Most fibers in both AFG and AFG/fSAP hydrogels displayed an oriented distribution with a percentage of 42.03% and 43.95%, respectively, indicating that the combination of SAP had no negative effect on the orientation of the original fibrin hydrogel (Fig. 2C). In addition, the AFG/fSAP hydrogel exhibited significantly higher water content than AFG hydrogel (Fig. 2D).

The morphology and internal composition of the hydrogels were observed using SEM and TEM. The intrinsic fibrillogenesis of fibrin resulted in the formation of linear fibrin fibrils with diameters of approximately 100 nm, while the diameter of the SAP nanofibers ranged from 15 nm to 30 nm, as previously reported [31,46]. SEM images showed the aligned fibers in both AFG and AFG/fSAP hydrogels (Fig. 2E). In AFG, the surface of the fibers was smooth and uniform, while the aligned fibrin fibers in AFG/fSAP were obviously surrounded by dense nanofibers of fSAP, leading to a rough surface. The diameters of surrounding SAP nanofibers were 17.78 ± 3.03 nm according to the pictures, consistent with reported data. The distribution frequencies of fiber directions are analyzed by defining the longitudinal axis of the samples as the reference direction (Fig. S1A). The fibers of AFG were distributed between −10° and 10°, while the fibers of AFG/fSAP were distributed between −15° and 15°, indicating that the addition of fSAP had only a slight effect on the alignment of primary fibrin nanofibers, in accordance with the micro-CT results. TEM images showed the cross-sectional microstructure of the nanofibers in AFG and AFG/fSAP hydrogels (Fig. 2F). The fibers in AFG exhibited a compact structure with diameters distributed between 100 nm and 400 nm, while the fibers in AFG/fSAP showed a porous structure composed of numerous nanofibers with increased diameters distributed between 250 nm and 650 nm (Fig. S1B). These results indicated that the fSAP nanofibers are distributed both on the surface and in the interior of AFG nanofibers. Additionally, the ubiquitous fSAP nanofibers strengthened the connection among adjacent fibrin fibers through a thin fibrous layer. The mean fiber diameter of AFG/fSAP (408.78 ± 98.18 nm) was significantly larger than that of AFG (237.18 ± 67.71 nm, $P < 0.01$, Fig. S1C).

The rheological measurements and AFM-based force mapping were performed to examine the stiffness and viscoelasticity properties of AFG and AFG/fSAP hydrogels. As shown in Fig. 2G, the storage modulus (G′) and loss modulus (G″) of the hydrogels remained steady under a constant 1% deformation at frequencies from 0.010 to 1.259 Hz, with G′ much larger than G″, suggesting that the hydrogels were viscoelastic solid, while the fSAP hydrogels exhibited similar properties to AFG and fSAP hydrogels according to previous study [46]. At 1 Hz of frequency (Fig. 2H), the average G′ values of the AFG (1811.77 ± 275.71 Pa) and AFG/fSAP (1336.07 ± 266.60 Pa) hydrogels were not significantly different, both of which were lower than those of the fSAP hydrogels (~3.0 kPa). However, the average G″ value of AFG/fSAP hydrogel (125.76 ± 20.66 Pa) was significantly lower than those of the AFG hydrogel (332.89 ± 50.49 Pa, $P < 0.01$) and fSAP hydrogels, indicating the decreased viscosity of AFG/fSAP hydrogel. The G″ values of all hydrogels were approximatively 10%–20% of their G′ values, indicating a similar property to the viscoelastic nerve tissue [27]. The Young's moduli of AFG and AFG/fSAP hydrogels were 3.11 ± 0.34 kPa and 2.72 ± 0.29 kPa, respectively, without significantly difference (Fig. 2I). In the process of peripheral nerve repair, SCs and regenerated neurites can sense the stiffness of the surrounding matrix, which affects the cell fate and neurite elongation [53]. The investigation on the mechanical response of neural cells to matrix stiffness suggested that the neurites had a preferential orientation towards collagen gels stiffer than 2 kPa and softer than 10 kPa [54]. Silk hydrogels with stiffness of 7.4 kPa and 22.4 kPa could greatly promote the neurite extension of chick dorsal root ganglion (DRG) [55]. DRGs on fibrin gels with compressive modulus of 2.5 kPa exhibited longer neurite extension compared with those on stiffer fibrin gels [56]. These results indicated that the AFG/fSAP hydrogel possessed an appropriate stiffness and viscoelasticity properties close to those of the nerve tissue, and had the potential to promote neurite growth.

Based on the hydrophobic properties of fibrin and strong hydrophilicity of self-assembling peptides, we speculated that the chemical groups on the surface of AFG interacted with the corresponding groups of the self-assembling peptides, leading to increased hydrophilicity in AFG/fSAP compared with the hydrophobic AFG, thus changing the light transmittance of the hydrogel [57]. The self-assembling peptides introduced more water into the hydrogel, causing significantly higher water content in AFG/fSAP compared to AFG, which stretched the nanofiber network and increased the volume of AFG/fSAP. To verify our hypothesis, the docking study of AFG and fSAP was conducted to illustrate their

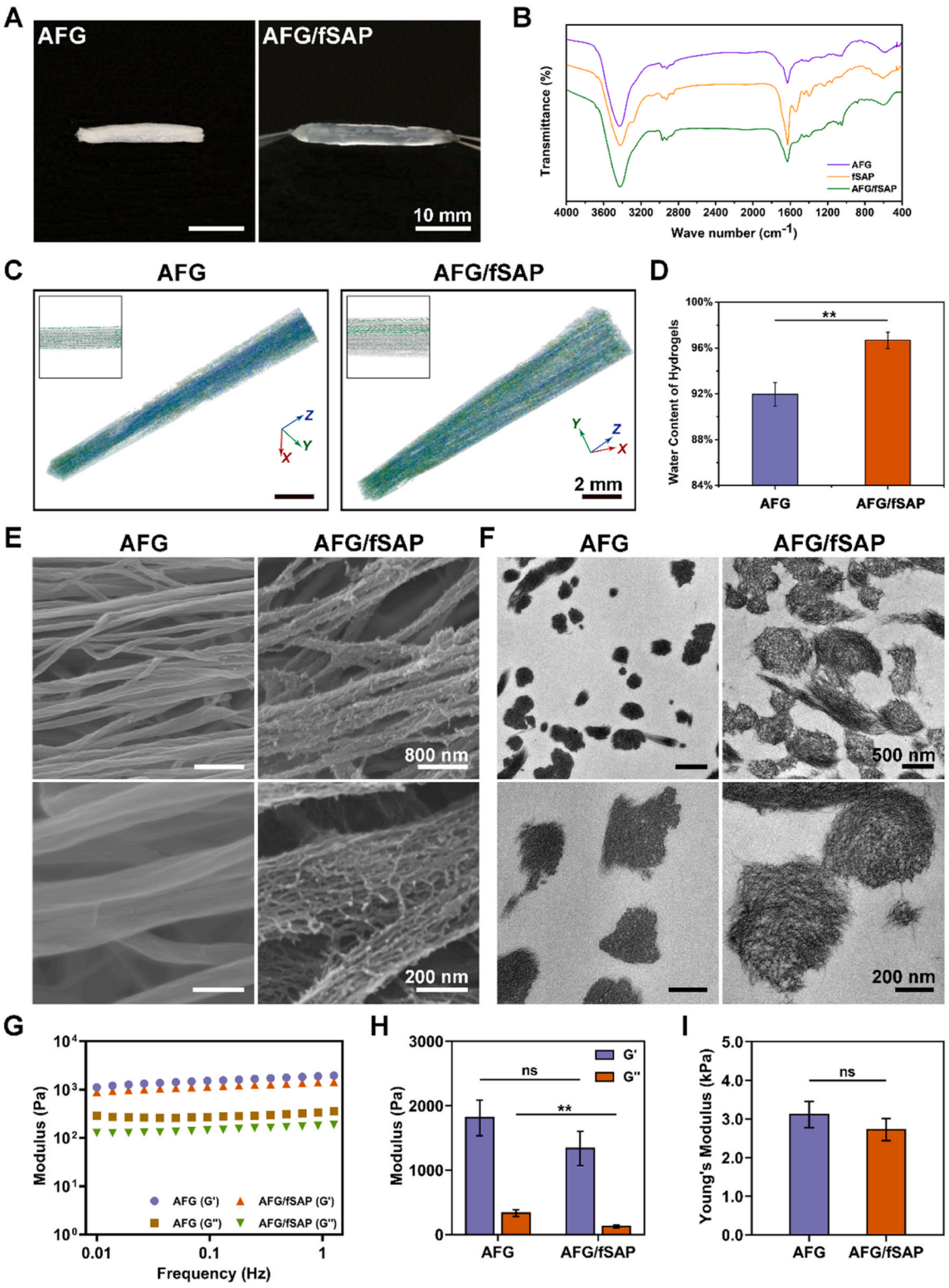

Fig. 2. Characterization of the AFG and AFG/fSAP hydrogels. (A) Images of AFG and AFG/fSAP hydrogels. (B) The representative FTIR spectra of AFG and AFG/fSAP hydrogels. (C) Micro-CT images and the orientation analysis of AFG and AFG/fSAP hydrogel. (D) The water content of AFG and AFG/fSAP hydrogels. (E) SEM images of the longitudinal fracture surfaces of AFG and AFG/fSAP hydrogels. (F) TEM images of the transverse sections of AFG and AFG/fSAP hydrogels. (G) Rheological measurements of storage (G′) and loss (G″) moduli of AFG and AFG/fSAP hydrogels as function of the frequency (from 0.010 to 1.259 Hz) in a constant 1% strain mode. (H) The average G′ and G″ of AFG and AFG/fSAP hydrogels at 1 Hz. (I) Young's moduli of AFG and AFG/fSAP hydrogels measured by AFM. $^{**}P < 0.01$ (n = 3).

interactive ability (Fig. 3A). The simulation results demonstrated the non-covalent bonding interaction forces between fibrinogen and self-assembling peptides used in this study, for instance, hydrogen bonds and electrostatic forces, which mainly originated from the C═O and NH_2 groups in different amino acids (Fig. 3B and C). The ^1H NMR spectra of fSAP, fibrinogen, and their mixture in deuteroxide showed that the fibrinogen had a relatively strong peak at 3.4890 ppm, which was downfield shifted to 3.6058 ppm in the mixture (Fig. S2). Other relatively weak peaks at 2.4054 and 2.4309 ppm in the fibrinogen also disappeared in the mixture, indicating changes in the chemical environment around related hydrogen atoms caused by molecular interaction. Considering that no covalent bonds formed during the fabrication, the changes of peaks were mainly caused by the weak intermolecular interaction and the formation of non-covalent bonds between fSAP and fibrinogen, which indirectly reflected the molecular interaction fSAP and AFG. These results were consistent with those of FTIR analysis. Further, their combination increased the number of hydrophilic groups and contributed to the higher water content, which could facilitate cell adhesion and migration. However, one major concern is that the non-covalent bonds between AFG and peptides are relatively weak compared with covalent bonds. The manipulation during hydrogel fabrication is slow and gentle to avoid the suddenly dramatic change of the environment around the hydrogel. In addition, the peptide nanofibers can twist around the fibrin nanofibers, forming interpenetrating networks, which contributed to stabilize the combination. The SEM and TEM images confirmed that the binding could remain stable in AFG/fSAP hydrogel preparation. Additionally, the hydrogel was loaded in chitosan tubes for *in vivo* study, which offered a relatively closed space for maintaining the peptides and fibrin molecules. Therefore, the non-covalent binding between fSAP and AFG could provide enough binding force to maintain the stability of the composite hydrogel during hydrogel processing and *in vivo* application. However, it's noted that the peptide nanofibers could gradually release from the hydrogel when keeping in equilibrium solution or *in vivo* for a long period, which is a general degradation process and has no negative impact on the function of hydrogel.

To evaluate the *in vivo* degradation properties of the hydrogels, AFG and AFG/fSAP hydrogels with Cy5 were implanted subcutaneously in rats for two weeks (Fig. S3A). The fluorescence intensities in both AFG and AFG/fSAP decreased gradually from 1 to 14 days, with most of the fluorescence disappearing after 7 days, indicating that the hydrogels degraded after 7 days (Fig. 3D). At 7 and 14 days after surgery, the

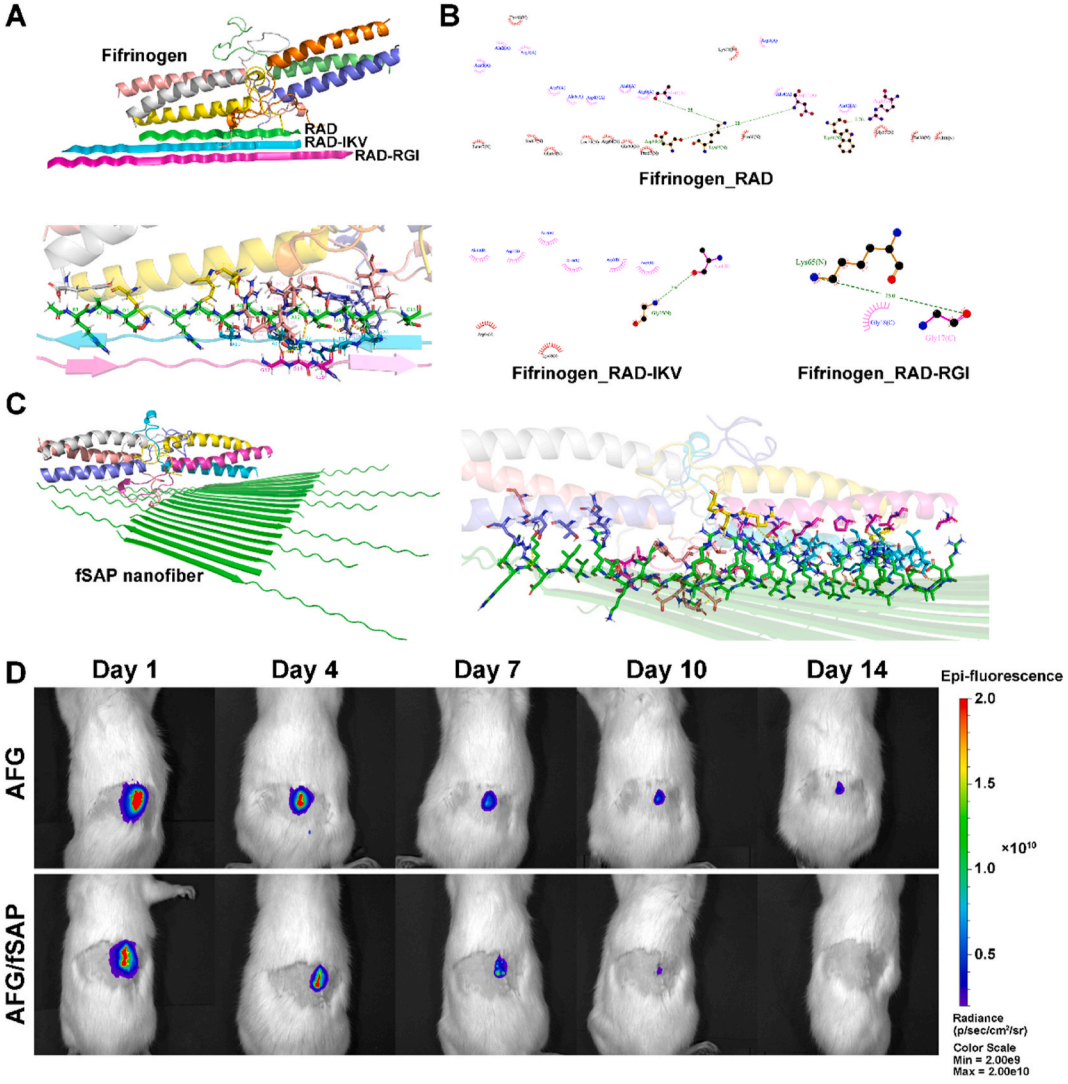

Fig. 3. Molecular docking simulation of the SAP with fibrinogen and the degradation performance of AFG and AFG/fSAP hydrogels *in vivo*. (A) The simulation analysis of fibrinogen with RAD, RAD-IKV, and RAD-RGI. (B) The simulation analysis of fibrinogen with RAD, RAD-IKV, and RAD-RGI, respectively. (C) The simulation analysis of fibrinogen with an fSAP nanofiber. (D) The representative fluorescence images of AFG and AFG/fSAP at 1, 4, 7, 10, and 14 days after subcutaneous implantation in rats (n = 3).

implants and the adjacent skin were retrieved for observation (Fig. S3B). At 7 days, the AFG was hard to identify, leaving a region with blood, while AFG/fSAP was still visible with both ends of the hydrogel scattered and partially degraded. This observation was in accordance with the fluorescence intensities at 7 days, when the AFG/fSAP showed an obviously higher intensity than AFG. At 14 days, no hydrogel was found in either AFG or AFG/fSAP group; however, the inner surface of the skin in AFG/fSAP group was smooth while a region with blood was still observed in AFG group probably caused by inflammation, which may lead to the weak fluorescence intensity at 14 days in AFG group. These results indicated that the hydrogels could degrade in 14 days. The degradation rate of hydrogels in NGCs is critical for nerve regeneration; it is essential that there be a balance between the rates of nerve regeneration and degradation, for maintaining structural integrity while minimizing unwanted compression damage [58]. In NGCs, nerves roughly regenerate at the rate of 1 mm per day, implying that the hydrogels inside the NGCs should completely degrade in 2 weeks, which was satisfied by the AFG/fSAP hydrogel [42]. According to previous studies, the fSAP hydrogels also showed progressive degradation because of the complex microenvironment with the changing pH, ionic strength, and enzymes *in vivo* [44,59,60]. The degradation of AFG and fSAP hydrogels was achieved by different means. The AFG hydrogel was degraded mainly by plasmin as well as matrix metalloproteases which were secreted by cells and widely distributed throughout the body [61]. Nevertheless, for fSAP hydrogels which were not provided with any specific enzyme site, the degradation was mainly accompanied by the disintegration and fragmentation of hydrogels and the release of peptides. Therefore, both the fSAP and AFG hydrogels exhibited good biodegradability *in vivo*. Based on the results, a subtle difference of degradation rate between AFG and AFG/fSAP was observed. Considering the different properties of AFG/fSAP compared to AFG, such as higher water content and changed microstructure, this phenomenon might be the result of multiple factors. These results indicated that the AFG/fSAP hydrogel possessed suitable degradation properties for nerve repair.

The modification of fibrin was carried out via different methods, for example, adding other components in the fibrin hydrogel and crosslinking with genipin [62]. Growth factors, such as VEGF and BDNF, could be incorporated directly into the fibrin matrices for tissue repair, but the release rate was hard to control, which limited the therapeutic efficacy *in vivo* [63]. Exogenous peptides or recombinant VEGF could be incorporated into fibrin matrices through a specific sequence, NQEQVSPL, by crosslinking with Factor XIIIa during the process of coagulation [64,65]. Inherent *knob:hole* interactions could also be used to modify fibrinogen or fibrin with various synthetic *knob A* mimics [66]. These attempts endowed fibrin with many other biological functions. However, the methods were limited by the strict reaction conditions that were not compatible for the electrospinning technique. In addition, the use of chemical crosslinking agents may sometimes introduce cytotoxicity and be detrimental for the function of fibrin hydrogel, which is not conducive to cell survival and tissue regeneration [67]. Moreover, simply combining growth factors or functional peptides only provides biological cues to fibrin hydrogel, which lacks the indispensable orientation cue for nerve repair. Therefore, the interpenetrating AFG/fSAP hydrogel is superior in providing both the necessary cues for nerve regeneration.

3.2. AFG/fSAP hydrogel induced Schwann cell alignment and enhanced neurotrophin secretion

SCs take a significant part in the reconstruction of injured nerves by wrapping around the neuronal axons to form compact myelin sheaths and secreting various neurotrophic molecules to promote axon growth [68,69]. To evaluate the impact of fiber alignment and bioactive motifs on SCs, we seeded primary SCs on pure AFG and AFG/fSAP hydrogels, and investigated their morphology and secretion of CNTF, BDNF, and NGF. After 3-day culture, the morphology of SCs were examined under a confocal microscope (Fig. 4A). S100 and p75 protein were employed as two markers for the identification of SCs [70]. TCP is used as a control group to show the effects of the 3D aligned structures of AFG and AFG/fSAP. The cells showed random cytoskeleton morphology on TCP, while they exhibited highly directionally aligned topography along the direction of the fibers on both AFG and AFG/fSAP hydrogels, indicating that the combination of self-assembling peptides had little impact on the alignment of the original fibrin fibers. This was consistent with other reports demonstrating that the aligned fibers are superior in inducing cell orientation that promotes SC maturation and myelination [15]. Additionally, the hydrogels were gradually degraded with the growth of SCs. The cells not only adhered to the surface of the hydrogel, but also degraded the hydrogel underneath and extended inside, contributing to the formation of a Schwann cell band for replacing the aligned fibers and providing an appropriate extracellular matrix, which is similar to the process of nerve regeneration *in vivo* (Fig. S4) [29].

Among various neurotrophic factors that are conducive for nerve regeneration, NGF improves sensorimotor recovery and directs axon elongation, while CNTF increases the myelin protein expression and facilitates the maturation of SCs. Meanwhile, BDNF has protective effects on neuronal survival following injury [8,71,72]. The secretion of CNTF, BDNF, and NGF by primary SCs on AFG and AFG/fSAP hydrogels after 3-day culture was significantly higher than that on TCP ($P < 0.05$ or $P < 0.01$, Fig. 4B), indicating that the aligned fibrin fiber enhanced the secretion function of SCs, consistent with reported data [73]. In addition, the secretion of these three neurotrophins on AFG/fSAP hydrogel was significantly higher than that on pure AFG hydrogel, indicating a positive effect of the functional motifs on SC secretion, as verified in our earlier study [46]. Therefore, the combination of aligned fibrin and self-assembling peptide could synergistically promote the directional arrangement and neurotrophin secretion of SCs, which would further guide the axonal extension during nerve regeneration [74].

3.3. AFG/fSAP hydrogel promoted axonal regeneration and re-myelination

Four groups of nerve grafts (Hollow, AFG, AFG/fSAP, and Autograft) were implanted to bridge the 15-mm-long transected sciatic nerve gaps in rats to evaluate the impact of the interpenetrating hydrogel on nerve regeneration *in vivo* (Fig. S5). The regenerated nerves with conduits in all groups were harvested and cut transversely at the distal site for the evaluation of axon regrowth and re-myelination at 12 weeks postoperatively (Fig. 5A). The toluidine-blue stained images revealed that uniform myelinated nerve fibers were successfully regenerated in all groups at 12 weeks postoperatively. Quantitative analysis suggested that the AFG/fSAP group (10682.2 ± 332.7 nerves/mm^2) had a significantly higher density of myelinated nerve fibers than the AFG (7814.3 ± 777.2 nerves/mm^2) and Hollow groups (6155.1 ± 469.9 nerves/mm^2, $P < 0.01$), approaching the Autograft group (12194.2 ± 644.9 nerves/mm^2) but with significant difference ($P < 0.01$). Furthermore, the nerve fiber density in AFG group was significantly higher than that in the Hollow group ($P < 0.01$), and both AFG and Hollow groups had significantly lower densities than the Autograft group ($P < 0.01$, Fig. 5B). The TEM images revealed more details in nerve conduction velocity maturity and myelination degree of regenerated nerves that are indicated by axonal area and myelin sheath thickness [75]. Both the nerve fiber diameter (6.03 ± 0.36 μm) and myelin sheath thickness (1.04 ± 0.15 μm) in the Autograft group were significantly larger than those in the other three groups ($P < 0.01$ or $P < 0.05$, Fig. 5C and D). The mean diameter of myelinated nerve fibers in the AFG/fSAP group (5.30 ± 0.25 μm) was significantly larger than those in the Hollow (2.46 ± 0.13 μm, $P < 0.01$) and AFG (3.27 ± 0.24 μm, $P < 0.01$) groups, and the myelin sheath thickness in the AFG/fSAP group (0.73 ± 0.03 μm) was significantly larger than those in the Hollow (0.36 ± 0.04 μm, $P < 0.01$) and AFG

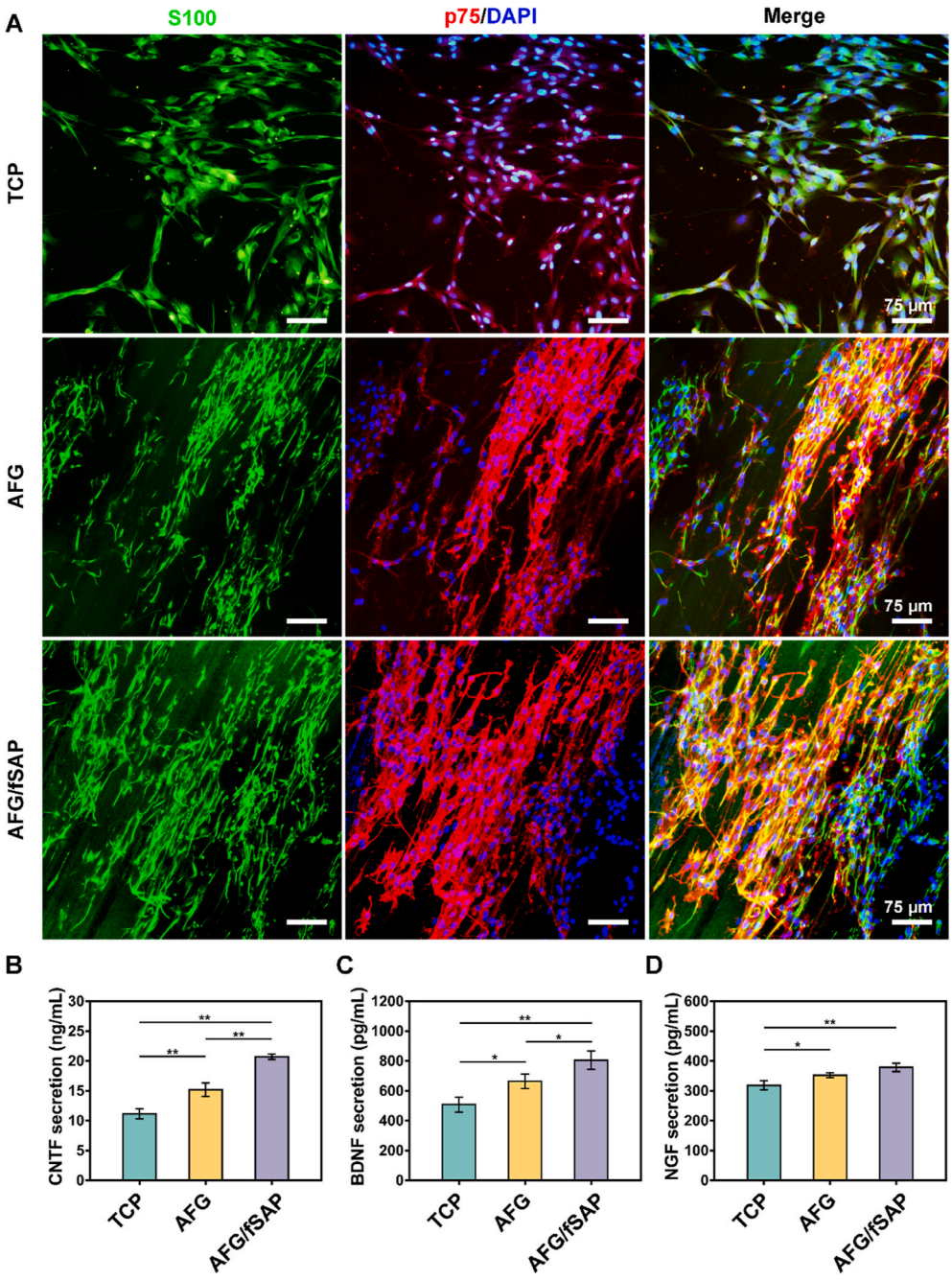

Fig. 4. Schwann cell morphology and neurotrophin secretion. (A) Representative confocal microscopy images of SCs stained with S100 (green) and p75 (red) on TCP, AFG and AFG/fSAP on day 3. The nuclei were stained with DAPI (blue). (B–D) The secretion of CNTF, BDNF, and NGF of SCs on TCP, AFG and AFG/fSAP after incubation for 3 days. $^{*}P < 0.05$ and $^{**}P < 0.01$ (n = 3).

(0.49 ± 0.03 μm, $P < 0.01$) groups, indicating promoted re-myelination via the synergistic effect of aligned fibrin fibers and functional motifs. Additionally, the myelin sheath thickness and nerve fiber diameter in the AFG group were significantly larger than those in the Hollow group, consistent with previous results [32]. Subsequently, the diameter/perimeter-based g-ratios were calculated to assess the degree of nerve fiber myelination. As previously reported, the optimal value of g-ratio in healthy peripheral nerves is approximatively 0.6 [76,77]. In this study, the average values of both g-ratios fluctuated between 0.6 and 0.7 in all groups, reflecting a generally completed myelination of the regenerated nerve fibers. The diameter-based g-ratio in the AFG/fSAP (0.67 ± 0.03) and AFG (0.62 ± 0.05) groups were significantly lower than that in the Hollow group (0.71 ± 0.02, $P < 0.01$), with no significant difference compared to that in the Autograft group (0.66 ± 0.06, $P > 0.05$, Fig. 5E). This indicated that the addition of filling materials to hollow NGCs could significantly enhance the myelination of axons with regard to a longer nerve defect. The perimeter-based g-ratio in the AFG/fSAP group (0.69 ± 0.03) was significantly lower than that in the Hollow group (0.71 ± 0.02, $P < 0.05$), with no significant difference compared that in other groups (Fig. 5F). The g-ratio analysis scatter plot distribution of the AFG/fSAP and Autograft groups showed more myelinated nerves in larger diameters compared to the Hollow and AFG groups (Fig. 5G). The fitting curve of the g-ratios in each group also revealed that the myelin degree of regenerative nerves in the AFG/fSAP group was closest to that in the Autograft group. Notably, the fitting curves of the AFG and AFG/fSAP groups cut across each other,

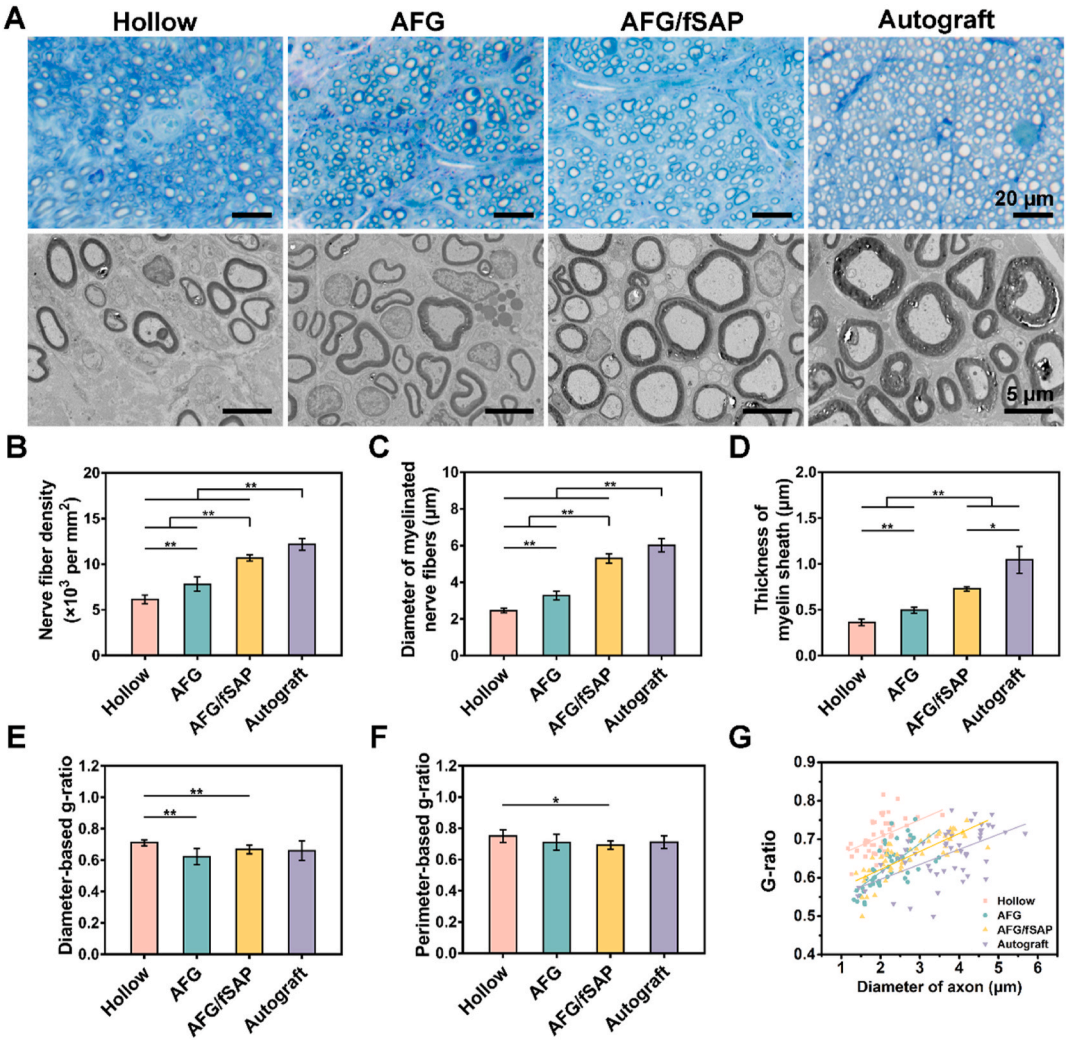

Fig. 5. Evaluation of regenerated nerve fibers at the distal site of nerve grafts at 12 weeks postoperatively. (A) Toluidine blue-stained images and TEM images of transverse sections at the distal site of the harvested nerve grafts. (B) Statistical analysis of the density of myelinated nerve fibers quantified from toluidine blue-stained images. (C) Statistical analysis of the diameter of the myelinated nerve fibers quantified from TEM images. (D) Statistical analysis of the thickness of the myelin sheath quantified from TEM images. (E) Statistical analysis of the diameter-based g-ratio. (F) Statistical analysis of the perimeter-based g-ratio. (G) The scatter diagram of g-ratio *versus* axon diameter. $^{*}P < 0.05$ and $^{**}P < 0.01$ (n = 5).

indicating that the AFG group had more myelinated nerves with small diameters and low g-ratio, which could grow further. In contrast, the axons in the Hollow group, mostly with small diameters, had higher g-ratios than those in the AFG group, suggesting that the myelination in the AFG group was more pronounced than that in the Hollow group. These results indicated that the aligned structure alone enhanced the nerve regrowth compared to hollow conduits, but the effect was insufficient and the combination with fSAP further promoted the regeneration. Therefore, the AFG/fSAP hydrogel greatly promote axon regeneration and myelination via the synergistic effect of aligned structure and biological stimulation.

3.4. AFG/fSAP hydrogel promoted nerve conduction recovery and motor function restoration

The recovery of nerve conduction and motor function is the ultimate goal of peripheral nerve regeneration, especially for longer nerve defects that take more time to regrow [78]. Electrophysiological examination was performed and the compound muscle action potential (CMAP) index was recorded to evaluate the recovery of nerve conduction at 12 weeks postoperatively [79]. The representative CMAP curves were displayed in Fig. 6A. The quantitative analysis revealed that the CMAP amplitude at the injured side in the AFG/fSAP group (11.86 ± 0.56 mV) was significantly higher than that in the Hollow (3.52 ± 0.44 mV, $P < 0.01$) and AFG (7.52 ± 0.53 mV, $P < 0.01$) groups, approaching that in the Autograft group (17.18 ± 1.09 mV, $P < 0.01$, Fig. 6B), indicating increased innervated muscle fibers in the AFG/fSAP group. Additionally, the CMAP latency in the AFG/fSAP group (1.64 ± 0.17 ms) was statistically higher than that in the Hollow (2.30 ± 0.12 ms, $P < 0.01$) and AFG (1.92 ± 0.19 ms, $P < 0.05$) groups, comparable to that of the Autograft group (1.48 ± 0.45 ms, $P > 0.05$), suggesting the comparable myelination degree in the AFG/fSAP group to that in the Autograft group (Fig. 6C). In addition, the regenerated nerves in the AFG group had significantly improved CMAP latency and amplitude than those in the Hollow group, suggesting the effect of AFG on recovered nerve activity. These results demonstrated that the aligned fiber and functional motifs had a synergistic effect in promoting the myelination of regenerated nerves and facilitating the conduction function recovery.

The function and structure of gastrocnemius muscle innervated by the sciatic nerve has a capacity to reflect the nerve regeneration degree. At 12 weeks postoperatively, the muscle atrophy in different groups was revealed in Masson's trichrome staining images of the gastrocnemius muscle (Fig. 7A). In the Hollow group, the muscle atrophy was severe with widely distributed collagen fibers (stained in blue), which was

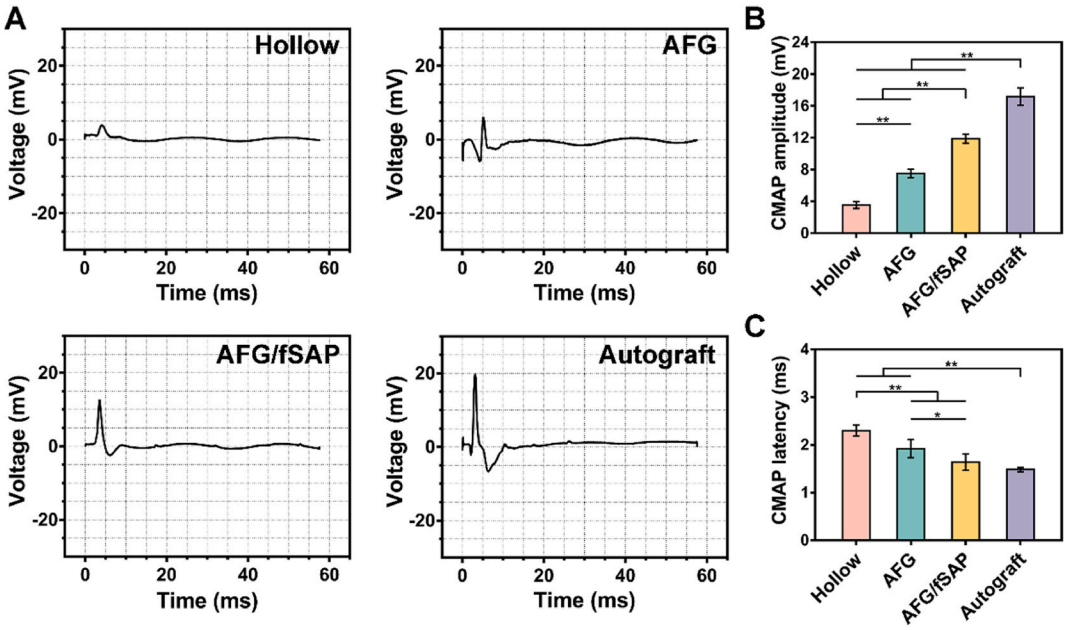

Fig. 6. Evaluation of electrophysiological performance at 12 weeks postoperatively. (A) Representative CMAP recordings at the injured side. Electrical stimulation (3.0 mA, 1 Hz, 0.1 ms) was applied at the proximal and distal nerve stumps. (B) Statistical analysis of CMAP amplitude at the injured side. (C) Statistical analysis of CMAP latency at the injured side. *$P < 0.05$ and **$P < 0.01$ (n = 5).

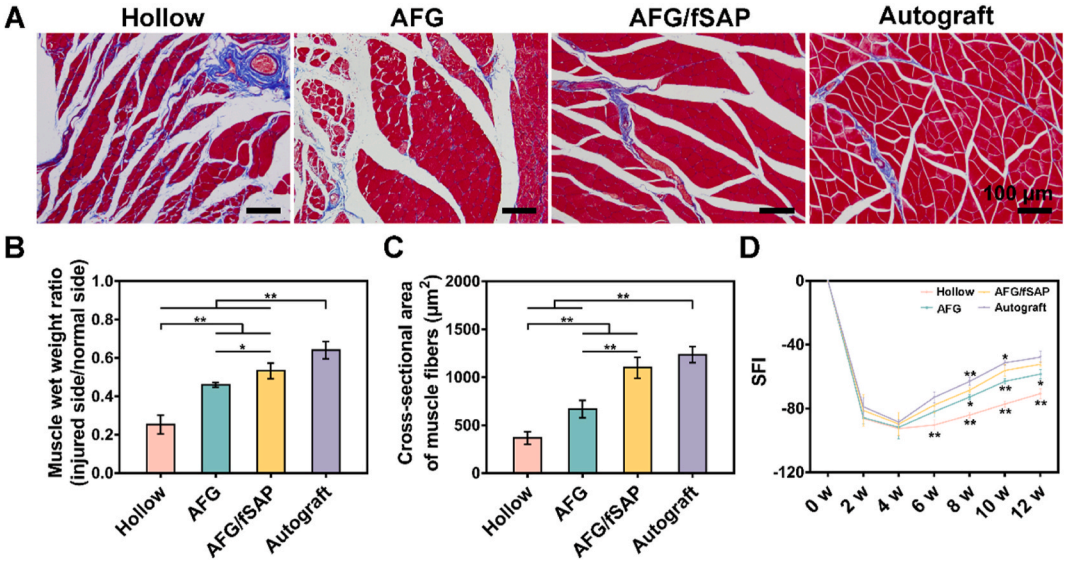

Fig. 7. Evaluation of motor functional recovery at 12 weeks postoperatively. (A) Masson's trichrome staining of the transverse sections of muscles from the injured limbs. (B) Statistical analysis of muscle wet weight ratios of the lesioned side of rats relative to the non-lesioned side. (C) Statistical analysis of the average cross-sectional areas of the muscle fibers. (D) SFI values over a 12-week observational period. *$P < 0.05$ and **$P < 0.01$ (n = 5).

improved with decreased collagen deposits in the AFG, AFG/fSAP, and Autograft groups. Interestingly, the muscles in the AFG/fSAP group exhibited an approximate morphology to those in the Autograft groups, with not significant atrophy. To quantitatively evaluate muscle atrophy, the muscle weight ratio was calculated by comparing the muscle at the lesioned side to that at the non-lesioned side (Fig. 7B). The muscle wet weight ratio in the AFG/fSAP group (53.29% ± 4.11%) was statistically higher than those in the Hollow (25.29% ± 4.82%, $P < 0.01$) and AFG (46.07% ± 1.25%, $P < 0.05$) groups, but significantly lower than that in the Autograft group (64.08% ± 4.48%, $P < 0.01$). In addition, statistical analysis indicated that the average cross-sectional area of gastrocnemius muscle fibers of the AFG/fSAP group (1100.72 ± 108.67 μm^2) was at an equivalent level to that of the Autograft group (1235.63 ± 84.60 μm^2, $P > 0.05$), significantly higher than those of the Hollow (366.81 ± 64.27 μm^2, $P < 0.01$) and AFG (667.76 ± 91.02 μm^2, $P < 0.01$) groups, suggesting promoted muscle re-innervation in the AFG/fSAP and Autograft groups (Fig. 7C).

Loss of nerve innervation and muscle atrophy induce a morbid gait of experimental rats. To evaluate the motor function recovery along nerve repair, walking track analysis was performed every 2 weeks post-operatively using the CatWalk system. The sciatic function index (SFI) was calculated from the footprints for evaluating sciatic nerve function [80]. SFI values approaching 0 indicate normal motor function, while SFI values approaching −100 suggest complete dysfunction. In all groups, SFI values decreased continuously in the initial 4 weeks after surgery, indicating the muscle denervation and the damaged motor

function caused by nerve transection in the early stage, which was consistent with previous studies [8]. After 4 weeks, SFI values exhibited an increasing trend from 6 weeks to 12 weeks, suggesting that the muscle regained innervation and started recovery because of the successful nerve regeneration (Fig. 7D). Significant difference was not found among groups at 2 or 4 weeks postoperatively ($P > 0.05$). At 6 weeks, SFI values of the AFG, AFG/fSAP, and Autograft groups were significantly higher than that of the Hollow group ($P < 0.01$). At 8 and 10 weeks, the SFI value of the AFG/fSAP group was statistically higher than those of the Hollow and AFG groups, but significantly lower than that of the Autograft group ($P < 0.05$ or $P < 0.01$). However, at 12 weeks, there was no significant difference between the AFG/fSAP and Autograft groups ($P > 0.05$), indicating that the AFG/fSAP hydrogel could have a comparable effect to autologous nerves on motor function recovery after a three-month repair period.

In general, the efficiency of repairing the sciatic nerve with AFG/fSAP hydrogel in the chitosan conduit was more satisfactory than with pure AFG and a hollow conduit. After 12 weeks, nerve conduction function and motor function were improved significantly, which was ideally comparable to those of autologous nerves. Although there were disparities in the number of innervated muscle fibers between the AFG/fSAP and Autograft groups, which might explain the lower muscle weight ratio in the AFG/fSAP group, the myelination degree and muscle fiber cross-sectional area of the AFG/fSAP group were comparable to those of the Autograft group, which could explain the superior SFI at 12 weeks. These combined results indicated that the AFG/fSAP hydrogel had a significant promoting effect on functional recovery for the treatment of sciatic nerve injury.

3.5. AFG/fSAP hydrogel upregulated regeneration-associated genes and activated the PI3K/Akt and MAPKs signal transduction pathways in vivo

The mechanism of nerve regeneration *in vivo* is reflected by the expression changes of abundant genes following PNI, with the quantity of differentially expressed genes reaching a maximum at one week postoperatively [81,82]. To investigate the mechanism of sciatic nerve regeneration induced by the AFG/fSAP hydrogel, the expression of regeneration-associated genes in nerve grafts was assessed by qRT-PCR at one week postoperatively. Generally, most of the regeneration-associated genes exhibited the highest expression in the Autograft group while the lowest in the Hollow group (Fig. 8A). Most of the evaluated genes in the AFG/fSAP group had higher expressions compared with those in the AFG and Hollow groups, especially VEGF, leukemia inhibitory factor (LIF), LN, GDNF, Gas6, PTN, BDNF, and CD31, which contributed to the angiogenesis, neuritogenesis and re-myelination [83–85]. Additionally, the expression of CNTF and NGF in the AFG/fSAP group was significantly higher than that in the AFG group, indicating the positive effect of functionalized SAP in neurotrophin secretion, which was consistent with the *in vitro* results ($P < 0.05$, Fig. 8B). Compared to the Hollow and AFG groups, the expression of BDNF was upregulated in the AFG/fSAP group, comparable to the Autograft group ($P > 0.05$). Moreover, upregulated expression of GDNF

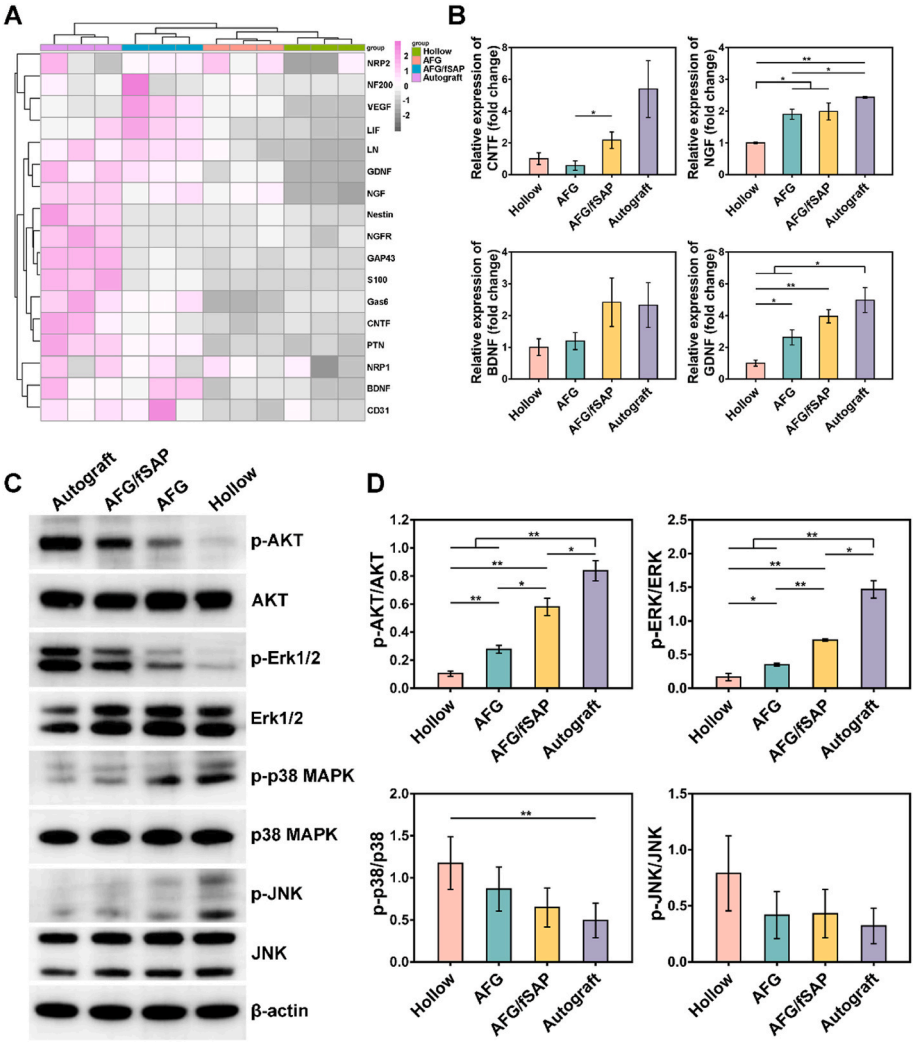

Fig. 8. Evaluation of the expression of regeneration-associated genes and activation of PI3K/AKT and MAPK pathways in different groups at 1 week postoperatively. (A) qPCR analysis of regeneration-associated genes. (B) Relative expression of CNTF, NGF, BDNF, and GDNF. (C) The protein levels of p-AKT, AKT, p-Erk1/2, Erk1/2, p-p38 MAPK, p38 MAPK, p-JNK, and JNK in regenerated sciatic nerves analyzed by Western blot. (D) Quantification analysis of the immunoblot data, with β-actin as the loading control. $^{*}P < 0.05$ and $^{**}P < 0.01$ (n = 3).

was observed in the AFG/fSAP and AFG groups compared with the Hollow group ($P < 0.05$). These results indicated that the AFG/fSAP hydrogel could promote nerve regeneration through the upregulation of neurotrophin expression.

The phosphatidylinositide-3-kinase/Akt (PI3K/Akt) and mitogen-activated protein kinases (MAPKs) signal pathways are considered important for regulating cell survival, proliferation, and differentiation during nerve regeneration [86,87]. To reveal the underlying mechanism through which AFG/fSAP promotes nerve regeneration, the expression levels of p-AKT, AKT, p-Erk1/2, Erk1/2, p-p38, p38, p-JNK, and JNK of the lesioned sciatic nerves at 7 days postoperatively were measured in each group by Western blot (Fig. 8C). PI3K/Akt and Extracellular signal-regulated kinase (Erk)/MAPK contribute to neuronal survival and axon regrowth mediated by neurotrophic factors, which are activated during the axonal regeneration processes. At 7 days after surgery, the AFG and AFG/fSAP hydrogels indicated prominent expression of p-AKT and p-Erk1/2 compared with the Hollow group, indicating the activation of AKT and Erk1/2. The quantitative results suggested that the levels of p-AKT and p-Erk1/2 in the AFG/fSAP group were significantly elevated compared with those in the Hollow and AFG groups ($P < 0.05$, Fig. 8D). In addition, the levels of p-AKT and p-Erk1/2 in the AFG group were significantly upregulated compared to those in the Hollow group ($P < 0.05$). Additionally, p38 MAPK and c-Jun N-terminal kinases (JNKs) pathways feature prominently in regulating inflammatory responses, axon regeneration and myelination. The downregulated levels of p-p38 and p-JNK observed in the AFG/fSAP and AFG groups compared with the Hollow group indicated the hydrogels could promote nerve regeneration via attenuating the activation of p38 MAPK and JNK signaling ($P > 0.05$, Fig. 8D).

The mechanism on how individual topographical or biochemical cues modulate cell behavior and nerve regeneration is well studied. Cell adhesion to the ECM transmits extracellular signals to cells via integrin receptors. The aligned collagen nanofibers promoted proliferation of neural progenitor cells via interacting with β1 integrin and upregulating Erk1/2 phosphorylation to activate the Erk/MAPK signaling pathway [88]. The RGI peptide was demonstrated to induce neurite outgrowth and promote neuronal survival by inducing phosphorylation of AKT and Erk1/2 [89]. Bioinformatics analysis has also revealed that the aligned fibrin hydrogel could direct the morphology of stem cells and promote the neural differentiation via the activation of MAPK and PI3K/Akt signaling pathways in our recent study. However, there are few investigations into the mechanism on how topography and biochemical cues synergistically induce peripheral nerve regeneration *in vivo*. In the present study, the AFG/fSAP hydrogel upregulated the phosphorylation of AKT and Erk1/2 and downregulated the phosphorylation of p38 and JNK compared with the Hollow and AFG groups, indicating the synergetic effects of fiber alignment and functional peptides. Our hypothesis portends that the AFG/fSAP hydrogel played two roles in regulating nerve regeneration. On the one hand, the nanofibers mimicking nerve ECM transmitted stimulation signals to the SCs and axons via integrins to induce axon elongation and myelination. On the other hand, the hydrogel upregulated the expression and secretion of endogenous neurotrophins such as NGF and BDNF to accelerate nerve regeneration, as demonstrated by the qPCR results. However, the results indicated an overall effect of the hydrogels *in vivo*, and further investigations are needed to better elucidate the mechanism underlying nerve repair induced by such types of materials.

On the whole, intraluminal filling materials reported in earlier studies generally lacked the integration of biochemical cues with aligned guidance. In this study, a novel interpenetrating hydrogel composed of aligned fibrin nanofibers and functionalized self-assembling peptide nanofibers was fabricated. The combination of the aligned structure and functional motifs resulted in improvements in the topographical and biochemical dimensions, reflecting more superiority in repairing nerve defects [35]. The aligned fibers of the hydrogel supply directional guidance to regulate the arrangement of SCs and regenerated neurites [13]. Based on an earlier work, the IKVAV and RGI peptides facilitated the maturation of SCs, contributing to the reconstruction of the Büngner bands in the process of nerve repair [46]. Furthermore, various bioactive small molecules can be easily integrated into the hydrogel to offer different functions for targeted and refined regeneration. Therefore, the AFG/fSAP interpenetrating hydrogel would be most likely to contribute to the repair of long-distance lesions in thick nerves or the spinal cord with its robust synergistic capacity. Future directions include optimization of the combination method between aligned fibrin and peptides or other small molecules, quantification of functional additives, and in-depth investigation into the mechanism underlying material-induced peripheral nerve regeneration.

4. Conclusion

We proposed a practical strategy to construct a composite hydrogel presenting both topographical and biochemical cues in the present study. The AFG/fSAP interpenetrating hydrogel possessed the advantages of two components. The aligned structure and neural tissue-like soft elastic properties were preserved, providing the topological guidance as well as substrate stiffness cues for SC migration and axon outgrowth. The addition of fSAP improved the water content of the interpenetrating hydrogel and supplied more adhesion sites for cells. The AFG/fSAP hydrogel could completely degrade in 14 days, offering guidance to SCs and neurites, with no hindrance in the later nerve extension. Additionally, this method enables conjugation and extension of various functional motifs, such as IKVAV, RGI, and KLT, to the RAD sequence in the AFG/fSAP, for different biological functions. The AFG/fSAP hydrogel with IKVAV and RGI motifs promoted the alignment morphology of primary SCs and the secretion of NGF, BDNF, and CNTF *in vitro*, and was applied as an intraluminal filling material for a chitosan nerve conduit to bridge a 15-mm gap sciatic nerve defect in rats *in vivo*. The AFG/fSAP hydrogel was demonstrated a satisfactory efficacy in promoting sciatic nerve regeneration by enhancing the growth and myelination of regenerated nerve fibers while accelerating recovery of motor functions. Restored motor functions facilitated by the AFG/fSAP hydrogel were comparable to those of autografts, which are known as the gold standard. Furthermore, the AFG/fSAP hydrogel effectively advanced axon growth via activating PI3K/Akt and MAPK signaling pathways. Collectively, our study demonstrates an inspiring strategy for the design of novel intraluminal filling materials for the regeneration of long-distance nerve injury.

CRediT authorship contribution statement

Shuhui Yang: Conceptualization, Methodology, Investigation, Validation, Formal analysis, Investigation, Writing – original draft, Writing – review & editing. **Jinjin Zhu:** Methodology, Investigation, Validation, Formal analysis, Writing – original draft, Writing – review & editing. **Changfeng Lu:** Methodology, Investigation, Validation, Formal analysis, Writing – original draft. **Yi Chai:** Methodology, Formal analysis, Writing – original draft. **Zheng Cao:** Conceptualization, Methodology, Investigation, Validation. **Jiaju Lu:** Methodology, Investigation, Validation. **Zhe Zhang:** Methodology, Investigation, Validation. **He Zhao:** Methodology, Investigation, Validation, Formal analysis. **Yin-Yuan Huang:** Methodology, Investigation, Validation, Formal analysis, Writing – review & editing. **Shenglian Yao:** Conceptualization, Methodology, Investigation, Validation, Funding acquisition. **Xiangdong Kong:** Supervision, Methodology, Investigation, Validation. **Peixun Zhang:** Supervision, Methodology, Investigation, Validation, Formal analysis, Resources, Project administration, Funding acquisition, Writing – original draft. **Xiumei Wang:** Supervision, Conceptualization, Methodology, Investigation, Validation, Formal analysis, Resources, Project administration, Funding acquisition, Writing – original draft, Writing – review & editing.

Declaration of competing interest

The authors declare that they have no known competing financial interests or personal relationships that could have appeared to influence the work reported in this paper.

Acknowledgements

We acknowledge the financial support from the National Key R&D Program of China (No. 2020YFC1107600, 2018YFB0704304, and 2018YFB1105504), Shandong Province Key R&D Program of China (No. 2019JZZY011106), the National Natural Science Foundation of China (No. 31771056 and 31800813), the Key Laboratory of Trauma and Neural Regeneration (Peking University), the Ministry of Education (No. BMU2019XY007-01), the Ministry of Education Innovation Program of China (No. IRT_16R01), and Shenzhen Science and Technology Program (No. 20190806162205278). We thank Prof. Jiang Peng and Prof. Yu Wang from Institute of Orthopedics, Chinese PLA General Hospital for the help with animal experiments. We thank Juncong Hong from The Second Affiliated Hospital Zhejiang University School of Medicine for the help with qPCR and Western blot. We also thank Yue Sun and Jingjing Wang at Center of Biomedical Analysis, Tsinghua University for the help with confocal microscopy. We also thank Junfei Huang at Shimadzu (China) Co., Ltd. for the help of technology and equipment of micro-CT. We would like to thank *Editage* (www.editage.com) for English language editing.

Appendix A. Supplementary data

Supplementary data related to this article can be found at https://doi.org/10.1016/j.bioactmat.2021.05.056.

References

[1] S. Yi, L. Xu, X. Gu, Scaffolds for peripheral nerve repair and reconstruction, Exp. Neurol. 319 (2019) 112761, https://doi.org/10.1016/j.expneurol.2018.05.016.
[2] X. Gu, F. Ding, Y. Yang, J. Liu, Construction of tissue engineered nerve grafts and their application in peripheral nerve regeneration, Prog. Neurobiol. 93 (2) (2011) 204–230, https://doi.org/10.1016/j.pneurobio.2010.11.002.
[3] D. Grinsell, C.P. Keating, Peripheral nerve reconstruction after injury: a review of clinical and experimental therapies, J. Biomed. Biotechnol. (4) (2014) 698256, 2014.
[4] Y.C. Lin, K.G. Marra, Injectable systems and implantable conduits for peripheral nerve repair, Biomed. Mater. 7 (2) (2012), 024102, https://doi.org/10.1088/1748-6041/7/2/024102.
[5] X. Gu, F. Ding, D.F. Williams, Neural tissue engineering options for peripheral nerve regeneration, Biomaterials 35 (24) (2014) 6143–6156, https://doi.org/10.1016/j.biomaterials.2014.04.064.
[6] M. Aikeremujiang, A. Qiang, Past, present, and future of nerve conduits in the treatment of peripheral nerve injury, BioMed Res. Int. (2015) 237507, https://doi.org/10.1155/2015/237507, 2015.
[7] R.G.C. De, R.J. Spinner, M.J.A. Malessy, M.J. Moore, E.J. Sorenson, B.L. Currier, M. J. Yaszemski, A.J. Windebank, Accuracy of motor axon regeneration across autograft, single-lumen, and multichannel poly(lactic-co-glycolic acid) nerve tubes, Neurosurgery 1 (2008) 144–155, https://doi.org/10.1227/01.NEU.0000335081.47352.78.
[8] G. Zhou, W. Chang, X. Zhou, Y. Chen, F. Dai, A. Anwar, X. Yu, Nanofibrous nerve conduits with nerve growth factors and bone marrow stromal cells pre-cultured in bioreactors for peripheral nerve regeneration, ACS Appl. Mater. Interfaces 12 (14) (2020) 16168–16177, https://doi.org/10.1021/acsami.0c04191.
[9] M. Saheb-Al-Zamani, Y. Yan, S.J. Farber, D.A. Hunter, P. Newton, M.D. Wood, S. A. Stewart, P.J. Johnson, S.E. Mackinnon, Limited regeneration in long acellular nerve allografts is associated with increased Schwann cell senescence, Exp. Neurol. 247 (2013) 165–177, https://doi.org/10.1016/j.expneurol.2013.04.011.
[10] M. Sarker, S. Naghieh, A.D. McInnes, D.J. Schreyer, X. Chen, Strategic design and fabrication of nerve guidance conduits for peripheral nerve regeneration, Biotechnol. J. 13 (7) (2018), e1700635, https://doi.org/10.1002/biot.201700635.
[11] L. Luo, Y. He, L. Jin, Y. Zhang, F.P. Guastaldi, A.A. Albashari, F. Hu, X. Wang, L. Wang, J. Xiao, L. Li, J. Wang, A. Higuchi, Q. Ye, Application of bioactive hydrogels combined with dental pulp stem cells for the repair of large gap peripheral nerve injuries, Bioact. Mater. 6 (3) (2021) 638–654, https://doi.org/10.1016/j.bioactmat.2020.08.028.
[12] S.M. Kim, M.S. Lee, J. Jeon, D.H. Lee, K. Yang, S.W. Cho, I. Han, H.S. Yang, Biodegradable nerve guidance conduit with microporous and micropatterned poly (lactic-co-glycolic acid)-accelerated sciatic nerve regeneration, Macromol. Biosci. 18 (12) (2018), e1800290, https://doi.org/10.1002/mabi.201800290.
[13] J. Wang, H. Xiong, T. Zhu, Y. Liu, H. Pan, C. Fan, X. Zhao, W.W. Lu, Bioinspired multichannel nerve guidance conduit based on shape memory nanofibers for potential application in peripheral nerve repair, ACS Nano 14 (10) (2020) 12579–12595, https://doi.org/10.1021/acsnano.0c03570.
[14] X. Hu, X. Wang, Y. Xu, L. Li, J. Liu, Y. He, Y. Zou, L. Yu, X. Qiu, J. Guo, Electric conductivity on aligned nanofibers facilitates the transdifferentiation of mesenchymal stem cells into Schwann cells and regeneration of injured peripheral nerve, Adv. Healthcare Mater. 9 (11) (2020), e1901570, https://doi.org/10.1002/adhm.201901570.
[15] J. Wang, Y. Cheng, H. Wang, Y. Wang, K. Zhang, C. Fan, H. Wang, X. Mo, Biomimetic and hierarchical nerve conduits from multifunctional nanofibers for guided peripheral nerve regeneration, Acta Biomater. 117 (2020) 180–191, https://doi.org/10.1016/j.actbio.2020.09.037.
[16] J. Scheib, A. Hoke, Advances in peripheral nerve regeneration, Nat. Rev. Neurol. 9 (12) (2013) 668–676, https://doi.org/10.1038/nrneurol.2013.227.
[17] S. Vijayavenkataraman, Nerve guide conduits for peripheral nerve injury repair: a review on design, materials and fabrication methods, Acta Biomater. 106 (2020) 54–69, https://doi.org/10.1016/j.actbio.2020.02.003.
[18] Y. Wang, Y. Zhang, X. Li, Q. Zhang, The progress of biomaterials in peripheral nerve repair and regeneration, J. Neurorestoratol. 8 (4) (2020) 252–269, https://doi.org/10.26599/jnr.2020.9040022.
[19] J. Moskow, B. Ferrigno, N. Mistry, D. Jaiswal, K. Bulsara, S. Rudraiah, S. G. Kumbar, Review: bioengineering approach for the repair and regeneration of peripheral nerve, Bioact. Mater. 4 (1) (2019) 107–113, https://doi.org/10.1016/j.bioactmat.2018.09.001.
[20] Y. Zhao, Y. Liang, S. Ding, K. Zhang, H.Q. Mao, Y. Yang, Application of conductive PPy/SF composite scaffold and electrical stimulation for neural tissue engineering, Biomaterials 255 (2020) 120164, https://doi.org/10.1016/j.biomaterials.2020.120164.
[21] L. Tian, M.P. Prabhakaran, S. Ramakrishna, Strategies for regeneration of components of nervous system: scaffolds, cells and biomolecules, Regen. Biomater. 2 (1) (2015) 31–45, https://doi.org/10.1093/rb/rbu017.
[22] K. Zhang, H. Zheng, S. Liang, C. Gao, Aligned PLLA nanofibrous scaffolds coated with graphene oxide for promoting neural cell growth, Acta Biomater. 37 (2016) 131–142, https://doi.org/10.1016/j.actbio.2016.04.008.
[23] T. Panciera, A. Citron, D. Di Biagio, G. Battilana, A. Gandin, S. Giulitti, M. Forcato, S. Bicciato, V. Panzetta, S. Fusco, L. Azzolin, A. Totaro, A.P. Dei Tos, M. Fassan, V. Vindigni, F. Bassetto, A. Rosato, G. Brusatin, M. Cordenonsi, S. Piccolo, Reprogramming normal cells into tumour precursors requires ECM stiffness and oncogene-mediated changes of cell mechanical properties, Nat. Mater. 19 (7) (2020) 797–806, https://doi.org/10.1038/s41563-020-0615-x.
[24] A. Gloria, T. Russo, U. D'Amora, M. Santin, R. De Santis, L. Ambrosio, Customised multiphasic nucleus/annulus scaffold for intervertebral disc repair/regeneration, Connect. Tissue Res 61 (2) (2020) 152–162, https://doi.org/10.1080/03008207.2019.1650037.
[25] S. Wang, D.H.R. Kempen, G.C.W. de Ruiter, L. Cai, R.J. Spinner, A.J. Windebank, M.J. Yaszemski, L. Lu, Molecularly engineered biodegradable polymer networks with a wide range of stiffness for bone and peripheral nerve regeneration, Adv. Funct. Mater. 25 (18) (2015) 2715–2724, https://doi.org/10.1002/adfm.201500105.
[26] J.B. Leach, X.Q. Brown, J.G. Jacot, P.A. Dimilla, J.Y. Wong, Neurite outgrowth and branching of PC12 cells on very soft substrates sharply decreases below a threshold of substrate rigidity, J. Neural. Eng. 4 (2) (2007) 26–34, https://doi.org/10.1088/1741-2560/4/2/003.
[27] O. Chaudhuri, J. Cooper-White, P.A. Janmey, D.J. Mooney, V.B. Shenoy, Effects of extracellular matrix viscoelasticity on cellular behaviour, Nature 584 (7822) (2020) 535–546, https://doi.org/10.1038/s41586-020-2612-2.
[28] M. Sameem, T.J. Wood, J.R. Bain, A systematic review on the use of fibrin glue for peripheral nerve repair, Plast. Reconstr. Surg. 127 (6) (2011) 2381–2390.
[29] W. Daly, L. Yao, D. Zeugolis, A. Windebank, A. Pandit, A biomaterials approach to peripheral nerve regeneration: bridging the peripheral nerve gap and enhancing functional recovery, J. R. Soc. Interface 9 (67) (2012) 202–221, https://doi.org/10.1098/rsif.2011.0438.
[30] J.S. Belkas, M.S. Shoichet, R. Midha, Peripheral nerve regeneration through guidance tubes, Neurol. Res. 26 (2) (2004) 151–160.
[31] S. Yao, X. Liu, S. Yu, X. Wang, S. Zhang, Q. Wu, X. Sun, H. Mao, Co-effects of matrix low elasticity and aligned topography on stem cell neurogenic differentiation and rapid neurite outgrowth, Nanoscale 8 (19) (2016) 10252–10265, https://doi.org/10.1039/c6nr01169a.
[32] J. Du, J. Liu, S. Yao, H. Mao, J. Peng, X. Sun, Z. Cao, Y. Yang, B. Xiao, Y. Wang, P. Tang, X. Wang, Prompt peripheral nerve regeneration induced by a hierarchically aligned fibrin nanofiber hydrogel, Acta Biomater. 55 (2017) 296–309, https://doi.org/10.1016/j.actbio.2017.04.010.
[33] S. Yao, S. Yu, Z. Cao, Y. Yang, X. Yu, H.Q. Mao, L.N. Wang, X. Sun, L. Zhao, X. Wang, Hierarchically aligned fibrin nanofiber hydrogel accelerated axonal regrowth and locomotor function recovery in rat spinal cord injury, Int. J. Nanomed. 13 (2018) 2883–2895, https://doi.org/10.2147/IJN.S159356.
[34] Z. Cao, S. Yao, Y. Xiong, Z. Zhang, Y. Yang, F. He, H. Zhao, Y. Guo, G. Wang, S. Xie, H. Guo, X. Wang, Directional axonal regrowth induced by an aligned fibrin nanofiber hydrogel contributes to improved motor function recovery in canine L2 spinal cord injury, J. Mater. Sci. Mater. Med. 31 (5) (2020) 40, https://doi.org/10.1007/s10856-020-06375-9.
[35] L. Zhu, S. Jia, T. Liu, L. Yan, D. Huang, Z. Wang, S. Chen, Z. Zhang, W. Zeng, Y. Zhang, H. Yang, D. Hao, Aligned PCL fiber conduits immobilized with nerve growth factor gradients enhance and direct sciatic nerve regeneration, Adv. Funct. Mater. 30 (39) (2020), https://doi.org/10.1002/adfm.202002610.

[36] C.R. Carvalho, W. Chang, J. Silva-Correia, R.L. Reis, J.M. Oliveira, J. Kohn, Engineering silk fibroin-based nerve conduit with neurotrophic factors for proximal protection after peripheral nerve injury, Adv. Healthcare Mater (2020), e2000753, https://doi.org/10.1002/adhm.202000753.
[37] W. Zhang, G. Zhou, Y. Gao, Y. Zhou, J. Liu, L. Zhang, A. Long, L. Zhang, P. Tang, A sequential delivery system employing the synergism of EPO and NGF promotes sciatic nerve repair, Colloids Surf., B 159 (2017) 327–336, https://doi.org/10.1016/j.colsurfb.2017.07.088.
[38] A.N. Moore, J.D. Hartgerink, Self-assembling multidomain peptide nanofibers for delivery of bioactive molecules and tissue regeneration, Acc. Chem. Res. 50 (4) (2017) 714–722, https://doi.org/10.1021/acs.accounts.6b00553.
[39] T.L. Lopez-Silva, C.D. Cristobal, C.S. Edwin Lai, V. Leyva-Aranda, H.K. Lee, J. D. Hartgerink, Self-assembling multidomain peptide hydrogels accelerate peripheral nerve regeneration after crush injury, Biomaterials 265 (2021) 120401, https://doi.org/10.1016/j.biomaterials.2020.120401.
[40] J. Lu, X. Sun, H. Yin, X. Shen, S. Yang, Y. Wang, W. Jiang, Y. Sun, L. Zhao, X. Sun, S. Lu, A.G. Mikos, J. Peng, X. Wang, A neurotrophic peptide-functionalized self-assembling peptide nanofiber hydrogel enhances rat sciatic nerve regeneration, Nano Res. (2018), https://doi.org/10.1007/s12274-018-2041-9.
[41] A. Zamuner, M. Cavo, S. Scaglione, G.M.L. Messina, T. Russo, A. Gloria, G. Marletta, M. Dettin, Design of decorated self-assembling peptide hydrogels as architecture for mesenchymal stem cells, Materials 9 (9) (2016), https://doi.org/10.3390/ma9090727.
[42] C. Lu, Y. Wang, S. Yang, C. Wang, X. Sun, J. Lu, H. Yin, W. Jiang, H. Meng, F. Rao, X. Wang, J. Peng, Bioactive self-assembling peptide hydrogels functionalized with brain-derived neurotrophic factor and nerve growth factor mimicking peptides synergistically promote peripheral nerve regeneration, ACS Biomater. Sci. Eng. 4 (8) (2018) 2994–3005, https://doi.org/10.1021/acsbiomaterials.8b00536.
[43] Y. Sun, W. Li, X. Wu, N. Zhang, Y. Zhang, S. Ouyang, X. Song, X. Fang, R. Seeram, W. Xue, L. He, W. Wu, Functional self-assembling peptide nanofiber hydrogels designed for nerve degeneration, ACS Appl. Mater. Interfaces 8 (3) (2016) 2348–2359, https://doi.org/10.1021/acsami.5b11473.
[44] X. Liu, X. Wang, A. Horii, X. Wang, L. Qiao, S. Zhang, F.Z. Cui, In vivo studies on angiogenic activity of two designer self-assembling peptide scaffold hydrogels in the chicken embryo chorioallantoic membrane, Nanoscale 4 (8) (2012) 2720–2727, https://doi.org/10.1039/c2nr00001f.
[45] J. Lu, X. Yan, X. Sun, X. Shen, H. Yin, C. Wang, Y. Liu, C. Lu, H. Fu, S. Yang, Y. Wang, X. Sun, L. Zhao, S. Lu, A.G. Mikos, J. Peng, X. Wang, Synergistic effects of dual-presenting VEGF- and BDNF-mimetic peptide epitopes from self-assembling peptide hydrogels on peripheral nerve regeneration, Nanoscale (2019), https://doi.org/10.1039/c9nr04521j.
[46] S. Yang, C. Wang, J. Zhu, C. Lu, H. Li, F. Chen, J. Lu, Z. Zhang, X. Yan, H. Zhao, X. Sun, L. Zhao, J. Liang, Y. Wang, J. Peng, X. Wang, Self-assembling peptide hydrogels functionalized with LN- and BDNF- mimicking epitopes synergistically enhance peripheral nerve regeneration, Theranostics 10 (18) (2020) 8227–8249, https://doi.org/10.7150/thno.44276.
[47] S. Zhang, X. Liu, S.F. Barreto-Ortiz, Y. Yu, B.P. Ginn, N.A. DeSantis, D.L. Hutton, W. L. Grayson, F.Z. Cui, B.A. Korgel, S. Gerecht, H.Q. Mao, Creating polymer hydrogel microfibres with internal alignment via electrical and mechanical stretching, Biomaterials 35 (10) (2014) 3243–3251, https://doi.org/10.1016/j.biomaterials.2013.12.081.
[48] J. Zhu, S. Yang, K. Cai, S. Wang, Z. Qiu, J. Huang, G. Jiang, X. Wang, X. Fang, Bioactive poly (methyl methacrylate) bone cement for the treatment of osteoporotic vertebral compression fractures, Theranostics 10 (14) (2020) 6544–6560, https://doi.org/10.7150/thno.44428.
[49] S. Zhang, Designer self-assembling peptide nanofiber scaffolds for study of 3-D cell biology and beyond, Adv. Canc. Res. 99 (2008) 335–362, https://doi.org/10.1016/S0065-230X(07)99005-3.
[50] X. Liu, X. Wang, X. Wang, H. Ren, J. He, L. Qiao, F.Z. Cui, Functionalized self-assembling peptide nanofiber hydrogels mimic stem cell niche to control human adipose stem cell behavior in vitro, Acta Biomater. 9 (6) (2013) 6798–6805, https://doi.org/10.1016/j.actbio.2013.01.027.
[51] Y. Gu, J. Zhu, C. Xue, Z. Li, F. Ding, Y. Yang, X. Gu, Chitosan/silk fibroin-based, Schwann cell-derived extracellular matrix-modified scaffolds for bridging rat sciatic nerve gaps, Biomaterials 35 (7) (2014) 2253–2263, https://doi.org/10.1016/j.biomaterials.2013.11.087.
[52] R. Pugliese, M. Maleki, R.N. Zuckermann, F. Gelain, Self-assembling peptides cross-linked with genipin: resilient hydrogels and self-standing electrospun scaffolds for tissue engineering applications, Biomater. Sci. 7 (1) (2018) 76–91, https://doi.org/10.1039/c8bm00825f.
[53] K. Franze, J. Guck, The biophysics of neuronal growth, Rep. Prog. Phys. 73 (9) (2010), https://doi.org/10.1088/0034-4885/73/9/094601.
[54] C. Kayal, E. Moeendarbary, R.J. Shipley, J.B. Phillips, Mechanical response of neural cells to physiologically relevant stiffness gradients, Adv. Healthcare Mater. 9 (8) (2020), e1901036, https://doi.org/10.1002/adhm.201901036.
[55] A.M. Hopkins, L. De Laporte, F. Tortelli, E. Spedden, C. Staii, T.J. Atherton, J. A. Hubbell, D.L. Kaplan, Silk hydrogels as soft substrates for neural tissue engineering, Adv. Funct. Mater. 23 (41) (2013) 5140–5149, https://doi.org/10.1002/adfm.201300435.
[56] A.J. Man, H.E. Davis, A. Itoh, J.K. Leach, P. Bannerman, Neurite outgrowth in fibrin gels is regulated by substrate stiffness, Tissue Eng. 17 (23–24) (2011) 2931–2942, https://doi.org/10.1089/ten.tea.2011.0030.
[57] L. Zhang, B. Casey, D.K. Galanakis, C. Marmorat, S. Skoog, K. Vorvolakos, M. Simon, M.H. Rafailovich, The influence of surface chemistry on adsorbed fibrinogen conformation, orientation, fiber formation and platelet adhesion, Acta Biomater. 54 (2017) 164–174, https://doi.org/10.1016/j.actbio.2017.03.002.
[58] L. Huang, L. Zhu, X. Shi, B. Xia, Z. Liu, S. Zhu, Y. Yang, T. Ma, P. Cheng, K. Luo, J. Huang, Z. Luo, A compound scaffold with uniform longitudinally oriented guidance cues and a porous sheath promotes peripheral nerve regeneration in vivo, Acta Biomater. 68 (2018) 223–236, https://doi.org/10.1016/j.actbio.2017.12.010.
[59] X. Wu, L. He, W. Li, H. Li, W.M. Wong, S. Ramakrishna, W. Wu, Functional self-assembling peptide nanofiber hydrogel for peripheral nerve regeneration, Regen. Biomater. 4 (1) (2017) 21–30, https://doi.org/10.1093/rb/rbw034.
[60] T.Y. Cheng, M.H. Chen, W.H. Chang, M.Y. Huang, T.W. Wang, Neural stem cells encapsulated in a functionalized self-assembling peptide hydrogel for brain tissue engineering, Biomaterials 34 (8) (2013) 2005–2016, https://doi.org/10.1016/j.biomaterials.2012.11.043.
[61] A.C. Brown, T.H. Barker, Fibrin-based biomaterials: modulation of macroscopic properties through rational design at the molecular level, Acta Biomater. 10 (4) (2014) 1502–1514, https://doi.org/10.1016/j.actbio.2013.09.008.
[62] T.C. Gamboa-Martinez, V. Luque-Guillen, C. Gonzalez-Garcia, J.L. Gomez Ribelles, G. Gallego-Ferrer, Crosslinked fibrin gels for tissue engineering: two approaches to improve their properties, J. Biomed. Mater. Res. 103 (2) (2015) 614–621, https://doi.org/10.1002/jbm.a.35210.
[63] M. Moritz, S. Pfeifer, E.R. Balmayor, R. Mittermayr, S. Wolbank, H. Redl, M. van Griensven, VEGF released from a fibrin biomatrix increases VEGFR-2 expression and improves early outcome after ischaemia-reperfusion injury, J. Tissue Eng. Regen. Med. 11 (7) (2017) 2153–2163, https://doi.org/10.1002/term.2114.
[64] J. Ishihara, A. Ishihara, K. Fukunaga, K. Sasaki, M.J.V. White, P.S. Briquez, J. A. Hubbell, Laminin heparin-binding peptides bind to several growth factors and enhance diabetic wound healing, Nat. Commun. 9 (1) (2018) 2163, https://doi.org/10.1038/s41467-018-04525-w.
[65] E. Guc, P.S. Briquez, D. Foretay, M.A. Fankhauser, J.A. Hubbell, W.W. Kilarski, M. A. Swartz, Local induction of lymphangiogenesis with engineered fibrin-binding VEGF-C promotes wound healing by increasing immune cell trafficking and matrix remodeling, Biomaterials 131 (2017) 160–175, https://doi.org/10.1016/j.biomaterials.2017.03.033.
[66] A.S. Soon, S.E. Stabenfeldt, W.E. Brown, T.H. Barker, Engineering fibrin matrices: the engagement of polymerization pockets through fibrin knob technology for the delivery and retention of therapeutic proteins, Biomaterials 31 (7) (2010) 1944–1954, https://doi.org/10.1016/j.biomaterials.2009.10.060.
[67] N. Gligorijevic, V. Sukalovic, A. Penezic, O. Nedic, Characterisation of the binding of dihydro-alpha-lipoic acid to fibrinogen and the effects on fibrinogen oxidation and fibrin formation, Int. J. Biol. Macromol. 147 (2020) 319–325, https://doi.org/10.1016/j.ijbiomac.2020.01.098.
[68] R. Li, D. Li, C. Wu, L. Ye, Y. Wu, Y. Yuan, S. Yang, L. Xie, Y. Mao, T. Jiang, Y. Li, J. Wang, H. Zhang, X. Li, J. Xiao, Nerve growth factor activates autophagy in Schwann cells to enhance myelin debris clearance and to expedite nerve regeneration, Theranostics 10 (4) (2020) 1649–1677, https://doi.org/10.7150/thno.40919.
[69] K.R. Jessen, R. Mirsky, A.C. Lloyd, Schwann cells: development and role in nerve repair, Cold Spring Harb Perspect. Biol. 7 (7) (2015) a020487, https://doi.org/10.1101/cshperspect.a020487.
[70] X. Sun, Y. Wang, Z. Guo, B. Xiao, Z. Sun, H. Yin, H. Meng, X. Sui, Q. Zhao, Q. Guo, A. Wang, W. Xu, S. Liu, Y. Li, S. Lu, J. Peng, Acellular cauda equina allograft as main material combined with biodegradable chitin conduit for regeneration of long-distance sciatic nerve defect in rats, Adv. Healthcare Mater. 7 (17) (2018), e1800276, https://doi.org/10.1002/adhm.201800276.
[71] Y. Cui, C. Lu, D. Meng, Z. Xiao, X. Hou, W. Ding, D. Kou, Y. Yao, B. Chen, Z. Zhang, J. Li, J. Pan, J. Dai, Collagen scaffolds modified with CNTF and bFGF promote facial nerve regeneration in minipigs, Biomaterials 35 (27) (2014) 7819–7827, https://doi.org/10.1016/j.biomaterials.2014.05.065.
[72] C.D. Lopes, N.P. Goncalves, C.P. Gomes, M.J. Saraiva, A.P. Pego, BDNF gene delivery mediated by neuron-targeted nanoparticles is neuroprotective in peripheral nerve injury, Biomaterials 121 (2017) 83–96, https://doi.org/10.1016/j.biomaterials.2016.12.025.
[73] J. Xue, J. Yang, D.M. O'Connor, C. Zhu, D. Huo, N.M. Boulis, Y. Xia, Differentiation of bone marrow stem cells into Schwann cells for the promotion of neurite outgrowth on electrospun fibers, ACS Appl. Mater. Interfaces 9 (14) (2017) 12299–12310, https://doi.org/10.1021/acsami.7b00882.
[74] Q. Min, D.B. Parkinson, X.P. Dun, Migrating Schwann cells direct axon regeneration within the peripheral nerve bridge, Glia 69 (2) (2021) 235–254, https://doi.org/10.1002/glia.23892.
[75] G.V. Michailov, M.W. Sereda, B.G. Brinkmann, T.M. Fischer, B. Haug, C. Birchmeier, L. Role, C. Lai, M.H. Schwab, K.A. Nave, Axonal neuregulin-1 regulates myelin sheath thickness, Science 304 (5671) (2004) 700–703, https://doi.org/10.1126/science.1095862.
[76] W.A.H. Rushton, A theory of the effects of fibre size in medullated nerve, J. Physiol. 115 (1) (1951).
[77] D. Finkelstein, T. Chomiak, B. Hu, What is the optimal value of the g-ratio for myelinated fibers in the rat CNS? A theoretical approach, PLoS One 4 (11) (2009), https://doi.org/10.1371/journal.pone.0007754.
[78] K.C. Santos Roballo, S. Dhungana, Z. Jiang, J. Oakey, J.S. Bushman, Localized delivery of immunosuppressive regulatory T cells to peripheral nerve allografts promotes regeneration of branched segmental defects, Biomaterials 209 (2019) 1–9, https://doi.org/10.1016/j.biomaterials.2019.04.015.
[79] N.B. Fadia, J.M. Bliley, G.A. DiBernardo, D.J. Crammond, K.G. Marra, Long-gap peripheral nerve repair through sustained release of a neurotrophic factor in nonhuman primates, Sci. Transl. Med. 12 (527) (2020), https://doi.org/10.1126/scitranslmed.aav7753 eaav7753.

[80] S. Das, M. Sharma, D. Saharia, K.K. Sarma, M.G. Sarma, B.B. Borthakur, U. Bora, Vivo studies of silk based gold nano-composite conduits for functional peripheral nerve regeneration, Biomaterials 62 (2015) 66–75, https://doi.org/10.1016/j.biomaterials.2015.04.047.
[81] R. Nagarajan, N. Le, H. Mahoney, T. Araki, J. Milbrandt, Deciphering peripheral nerve myelination by using Schwann cell expression profiling, Proc. Natl. Acad. Sci. U. S. A 99 (13) (2002) 8998–9003, https://doi.org/10.1073/pnas.132080999.
[82] S. Li, Q. Liu, Y. Wang, Y. Gu, D. Liu, C. Wang, G. Ding, J. Chen, J. Liu, X. Gu, Differential gene expression profiling and biological process analysis in proximal nerve segments after sciatic nerve transection, PLoS One 8 (2) (2013), e57000, https://doi.org/10.1371/journal.pone.0057000.
[83] A.E. Haggerty, M.R. Bening, G. Pherribo, E.A. Dauer, M. Oudega, Laminin polymer treatment accelerates repair of the crushed peripheral nerve in adult rats, Acta Biomater. 86 (2019) 185–193, https://doi.org/10.1016/j.actbio.2019.01.024.
[84] S. Rittchen, A. Boyd, A. Burns, J. Park, T.M. Fahmy, S. Metcalfe, A. Williams, Myelin repair in vivo is increased by targeting oligodendrocyte precursor cells with nanoparticles encapsulating leukaemia inhibitory factor (LIF), Biomaterials 56 (2015) 78–85, https://doi.org/10.1016/j.biomaterials.2015.03.044.
[85] J.A. Stratton, A. Holmes, N.L. Rosin, S. Sinha, M. Vohra, N.E. Burma, T. Trang, R. Midha, J. Biernaskie, Macrophages regulate Schwann cell maturation after nerve injury, Cell Rep. 24 (10) (2018), https://doi.org/10.1016/j.celrep.2018.08.004, 2561-2572 e2566.
[86] H. Huang, H. Liu, R. Yan, M. Hu, PI3K/Akt and ERK/MAPK signaling promote different aspects of neuron survival and axonal regrowth following rat facial nerve axotomy, Neurochem. Res. 42 (12) (2017) 3515–3524, https://doi.org/10.1007/s11064-017-2399-1.
[87] R. Li, Y. Li, Y. Wu, Y. Zhao, H. Chen, Y. Yuan, K. Xu, H. Zhang, Y. Lu, J. Wang, X. Li, X. Jia, J. Xiao, Heparin-poloxamer thermosensitive hydrogel loaded with bFGF and NGF enhances peripheral nerve regeneration in diabetic rats, Biomaterials 168 (2018) 24–37, https://doi.org/10.1016/j.biomaterials.2018.03.044.
[88] Y. Wang, M. Yao, J. Zhou, W. Zheng, C. Zhou, D. Dong, Y. Liu, Z. Teng, Y. Jiang, G. Wei, X. Cui, The promotion of neural progenitor cells proliferation by aligned and randomly oriented collagen nanofibers through beta1 integrin/MAPK signaling pathway, Biomaterials 32 (28) (2011) 6737–6744, https://doi.org/10.1016/j.biomaterials.2011.05.075.
[89] K. Fobian, S. Owczarek, C. Budtz, E. Bock, V. Berezin, M.V. Pedersen, Peptides derived from the solvent-exposed loops 3 and 4 of BDNF bind TrkB and p75(NTR) receptors and stimulate neurite outgrowth and survival, J. Neurosci. Res. 88 (6) (2010) 1170–1181, https://doi.org/10.1002/jnr.22285.